**Increased Millirobot Traction in Running and Jumping through Leg Spines**

by

Jessica Stephanie Lee

A dissertation submitted in partial satisfaction of the

requirements for the degree of

Doctor of Philosophy

in

Engineering - Mechanical Engineering

in the

Graduate Division

of the

University of California, Berkeley

Committee in charge:

Professor Ronald S. Fearing, Co-chair
Professor Alice M. Agogino, Co-chair
Professor Robert Full
Professor Dennis Lieu

Spring 2018

**Increased Millirobot Traction in Running and Jumping through Leg Spines**

## Abstract

Increased Millirobot Traction in Running and Jumping through Leg Spines

by

Jessica Stephanie Lee

Doctor of Philosophy in Engineering - Mechanical Engineering

University of California, Berkeley

Professor Ronald S. Fearing, Co-chair

Professor Alice M. Agogino, Co-chair

In this thesis leg spines have been used in a variety of systems including traction for horizontal running, and a gripping mechanism for jumping on inclines. These spines were inspired by collapsible leg spines found on insects and spiders that provide a passive mechanism for increased traction while running over complex terrain. I used this architectural advantage as biological inspiration to increase the traction with a VelociRoACH, a high speed terrestrial robot. These spines exhibited anisotropic properties in the fore-aft and lateral directions, with a 2:1 holding-to-release force ratio on corkboard (0.2 N to 0.1 N). This increase in effective friction coefficient at the foot-to-surface contact points increased the running speed on flat ground and 20° inclines and the maximum incline the robot can traverse by 10°. The VelociRoACH with spines is able to engage the surface and pull up to 0.36 N whereas without spines it slips while pulling 0.2 N, increasing the useful work in pulling a load. The spines also allow the robot to remain dynamically stable and resist torque disturbances.

After preliminary experiments using bio-inspired spines on the VelociRoACH, the various structures insects use to enhance interaction with the substrate during jumping were examined. The effectiveness of spines at the base of cricket tibia and attachment pads on tarsi were tested in providing traction on various surfaces by measuring jump kinetic energy using high-speed video. Both substrate and attachment structure significantly affected jump kinetic energy, but most significantly spines increased jumping performance by 82% on Styrofoam.

Inspired by crickets, similar experiments were performed on a 2.5g jumping robot for more controlled tests. The addition of spines increased jump kinetic energy on Styrofoam by 65% and doubled its jump distance to 40cm. Adding rubber attachment pads allowed the robot to jump on Teflon, increasing the kinetic energy from 0 to 7.8mJ. Leg spines appear critical for maximum jumping performance on surfaces that allow penetration and attachment pads can increase performance on smooth surfaces.

Lastly, spines were used in a gripper mechanism for the monopedal jumping robot, Salto, to reduce slip and provide adhesion capabilities. The mechanism pushes in angled spines along their length and is kinematically constrained to engage/disengage with leg crouch/extension. The resulting gripper introduces no new actuators, enables jumping on penetrable inclines up to 60°, as opposed to a rubber ball foot that works up to 20°, and enables static adhesion to hold 7.5 times the robot's weight from a ceiling.

Overall leg and foot spines have been shown to be an effective means of increasing performance in traction and jumping without requiring additional actuators, degrees of freedom, batteries or control. This is especially useful for small robots that have limited real estate and weight constraints. However, using spines as a passive mechanical solution for traction can be used in larger robots and other applications as well.

To my family and my partner.

Mom, Dad, and Bryan, you supported me 100%.
Ethan, you are amazing and inspire me to be better.

# Contents

# List of Figures

# List of Tables

# Acknowledgments

Many, many thanks to Prof. Ron Fearing for his support, guidance, advice, and feedback on this report and all the papers we have published so far. All of this work is based on the research presented at IEEE International Conference on Robotics and Automation (ICRA) 2015 [28], Climbing and Walking Robots and Support Technologies for Mobile Machines 2016 [29], Society for Integrative and Comparative Biology 2017 [30], and work submitted to ICRA 2018 [31]. Also, thank you to Prof. Robert Full and Kaushik Jayaram from the Poly-PEDAL Lab for their insights on cockroach leg spines. Thank you to Lisa Treidel and Rebecca M. Clark from the Williams Lab and Peter Oboyski from the Essig Museum of Entomology for providing test subjects. Thank you to Sun-Pill Jung and Gwang-Pil Jung for manufacturing and modeling support in the BioRobotics Lab. Thanks to the members of the Biomimetic Millisystems Lab for their helpful comments and discussions, especially Ethan Schaler for manufacturing support and photography, and Carlos Casarez and Justin Yim for their valuable insights and manufacturing help. A big thank you to Mark Plecnik, who was a co-first-author for the work submitted to ICRA 2018.

Jessica was supported by the National Science Foundation under IGERT Grant No. DGE-0903711, the National Science Foundation Graduate Research Fellowship, and by the Army Research Laboratory under the Micro Autonomous Systems and Technology Collaborative Technology Alliance.

# Part I

# Building More Capable Robots

# Chapter 1

# Motivation and Background

## 1.1 Robots Function on Simple Substrates

Fig. 1.1 shows the FEMA Urban Search and Rescue team searching for people in the aftermath of a tornado. In the Biomimetic Millisystems lab, researchers are trying to build more capable search and rescue robots so that people don't have to put themselves at risk in areas such as this where they could potentially injure themselves. Robots are useful because they can not only localize survivors, like dogs, but they can also provide an internal layout of the area. There are search and rescue robots available, but some only function on ideal surfaces [46] and others are so large they could crush the people they are trying to save [7]. In the lab researchers have developed disposable, cheap robots that can be quickly built so we can have hundreds of these and be able to find people in a larger area. These robots are also small, insect-like and have many applications due to the fact that they are easily transportable and able to access small spaces that larger robots cannot. Yet there are many challenges associated with small robots because their size limits the amount of onboard processing or batteries that can be used. By drawing inspiration from animals, robots can be designed to have added capabilities without expensive closed-loop control or heavy actuators and batteries. An example of a palm-sized robot is CRAM, which is able to successfully

Figure 1.1: FEMA Urban Search and Rescue (NE TF1) team members search house to house for survivors in tornado devastated neighborhood in Moore, Oklahoma. Taken from fema.gov.

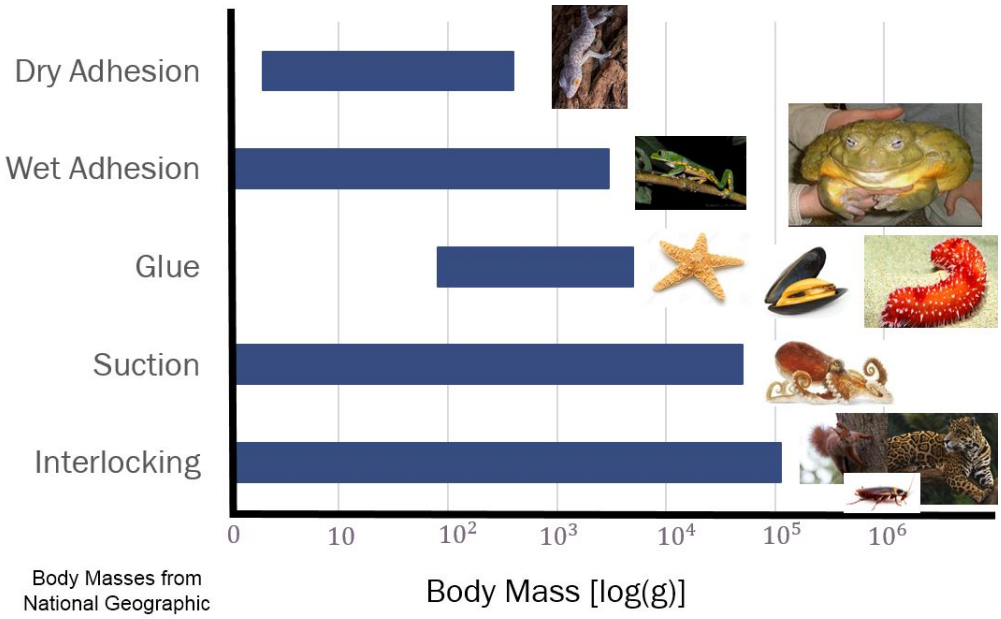


Figure 1.2: Different animal attachment mechanisms and their respective log body mass.

locomote after compressing its body in half [22]. The CRAM robot demonstrated that with medium ground friction it was able to achieve maximum speed. This is a step in the direction of making more capable robots, however this was in a controlled lab environment and investigating the interaction of legs with the environment is still needed.

There have been significant advancements in understanding locomotion on simple substrates, however current robots such as Stickybot [25], Atrius [42] and cheetah cub [45] have mainly been demonstrated on smooth clean glass, flat ground and high friction tracks. We've recently realized that to understand the structure and function of animal appendages and make more capable robots, we have to better characterize the interaction with the environment.

## 1.2 Animals Actively Engage Environment

Animals have a variety of ways to interact with substrates such as tree bark, wet branches and dirt [16]. Fig 1.2 shows a graph of animal attachment mechanisms and log body mass. Geckos use dry adhesion with one billion spatula on their toes using van der Waals forces [3]. Frogs use wet adhesion, which utilizes surface tension of water film between pad and surface [36]. Glue is used by mussels, starfish and sea cucumber, where they mix a hardener and resin, and can only be used once [27]. Octopus create a closed volume and produce negative pressure, however this requires a smooth surface [47]. Lastly we have interlocking through spines and claws which are used by animals such as leopards, cockroaches, and birds [16].

One body interlocks with another body when it either engages and fits into projections or recesses, or penetrates the other body to create its own hold surface in order to generate significant contact forces. Since interlocking seems to be the most versatile in body size and surface type, it could be a useful mechanism for many sizes of robot operating in different environments.

### Interlocking

There are many studies in biology on interlocking because there are so many different strategies. Snakes have ventral scales that have a significantly higher friction coefficient in the caudal than cranial direction [5]. Beetle tarsal claws can provide propulsive forces 10-20 times their average weight [10]. In lizards, one subcaudal scale can support 3.5-7 times its body weight [24]. Jayaram and Full found that cockroach leg spines can compensate for the lack of claws on rough surfaces [23].

### Choosing Spines

Out of these different body adaptations, I have chosen leg spines to study. In some insects they are collapsible which helps in loose substrates [43]. When the spines push into debris, they stiffen and provide traction, and as the legs pull out of debris the spines collapse inward and free themselves easily. They also work well in unclean environments, require no cleaning and can last many cycles. Spines have been shown to be useful in dynamic attachment during locomotion, such as jumping [16]. Engineered physical models have also been used in the past to show what makes good spines. For example, Asbeck and Cutkosky show that having multiple spines is a useful feature because then they are able to take on more load and that compliant spines allow load sharing. This means if it does not engage the first time, the compliance allows it to travel along a surface until it does. Spines also have an ideal tip radius that depends on the approach angle and surface roughness [1]. Bioinspired spines will allow robots to move in dirty, non-ideal environments, making more capable search and rescue robots.

## 1.3 Robots Using Spines

Substantial performance improvements have been achieved by several bio-inspired robots through passive mechanisms and smart mechanical design, such as spines used in terrestrial running [43], climbing [6][1][44][40][48][32], and perching [26][33][34]. Previous implementations capable of engaging and disengaging from a surface are shown in Fig. 1.3. Climbing robots quasi-statically engage vertical surfaces with cycle times comparable to a slow walk. Some examples of successful climbing robots are SpinyBotII [2], RiSE (Robots in Scansorial Environments) [44], and CLASH (Climbing Autonomous Sprawled Hexapod) [6]. SpinyBotII and RiSE draw inspiration from spines found on insect legs and use metal micro-hooks to

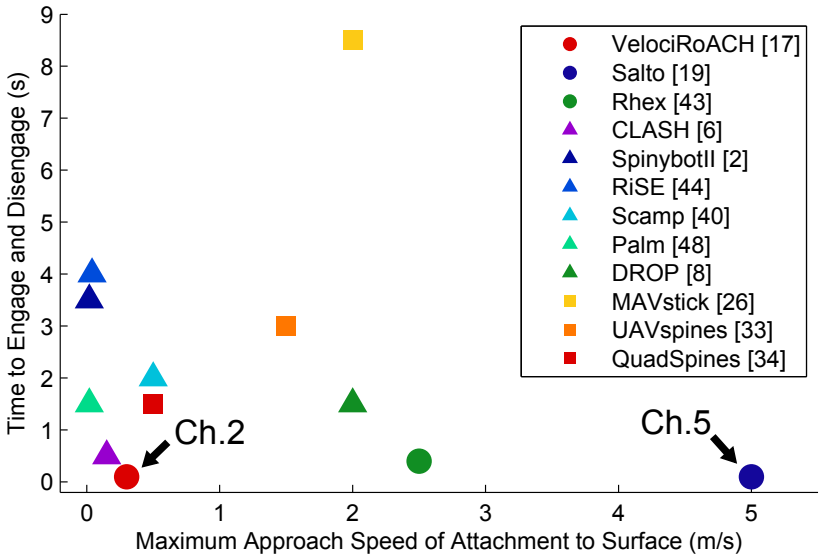


Figure 1.3: Comparison of previous applications of spines according to their approach speed to a surface and time to engage and disengage. Values were estimated if not immediately available. Terrestrial robots are circles, climbing robots are triangles, and perching mechanisms for flying robots are squares.

catch onto asperities in walls. CLASH uses passive self-stability and a remote center of compliance to engage and disengage its foot, similar to that found in geckos to climb faster. On the other extreme, flying robots equipped with perching mechanisms dynamically encounter surfaces, but are not designed to engage/disengage on a locomotive timescale. Little research on spine engagement has been performed in between these extremes. An outlier to these two groups is DROP, a climbing robot that utilizes multiples spines on a wheel to dynamically engage a surface and climb at high speeds [8].

The goal of my research is to improve traction for robots that operate on stance timescales shorter than perching robots but dynamically approach surfaces unlike climbing robots (Fig.1.3). A previous terrestrial robot utilizing spines is RHex (the Robot Hexapod) [43]. Designed to be a terrestrial robot, it utilized additional spikes at the bottom of its legs to be able to traverse surfaces that had low probability of foot contact, such as mesh. However, this was designed for a specific substrate, whereas the goal of the designs presented here will be to improve performance on a variety of substrates. First the preliminary research will be presented on spines for a terrestrial robot, VelociRoACH, which obtained higher speeds and walk-able incline angles through traction (Ch.2). Next it will be demonstrated how crickets utilize spines during jumping (Ch.3) and the first spines used on a jumping robot. The spines improved the horizontal jumping capabilities in a flea-inspired robot, but spines were only used during takeoff, since the robot could not make repeated jumps (Ch.4). All this research led to the work on the first spined gripper kinematically coupled to engage and disengage on an agile jumping robot (Ch.5).

# Chapter 2

# Leg Spines for Terrestrial Traction

## 2.1 Introduction

Preliminary research focused on a foot enhancement design inspired by the collapsible leg spines found on insects and spiders. These spines provide distributed mechanical feedback and are a passive mechanism for running over complex terrain. Anisotropic properties of spines permit engagement of the surface during thrust, but are easily disengaged during swing phase of gait because they collapse toward the leg as the leg slides forward [43]. The spines presented, unlike SpinyBotII, RiSE, and CLASH, are used here for traction on a minimally actuated robot to pull a load, not climb. Cooperative pulling by multiple robots has been explored as a method to maneuver objects [9], but here we examine the traction force limits of a single robot, and its energetic cost.

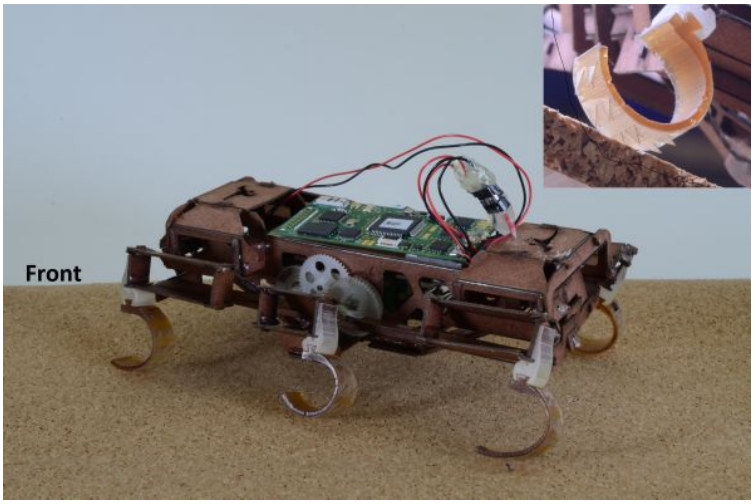


Figure 2.1: VelociRoACH with spines shown on cork board. (Upper Right) Expanded picture of the spines for reference.

## 2.2 Design

### Robot Platform

The robot used in this work, the VelociRoACH (Fig. 2.1), is one of the fastest legged running robots relative to its size (27 body-lengths/sec) [17]. This bio-inspired robot utilizes a hexapedal gait and C-legs, which provide distributed leg contact to help navigate uneven terrain. The VelociRoACH is 10 cm long with a mass of 30 g, and is driven by two DC motors, one for the left legs and the other for the right side. The body is constructed using the Smart Composite Microstructures Process (SCM) [20] and the dynamics were established from dynamic similarity scaling from a cockroach [17]. It should be noted that the C-legs are oriented in the opposite direction used in previous work [17] because spines create high pulling forces on the robot, which might cause the C-legs to buckle in the standard orientation. Additionally, we wanted the legs to be under tension while in thrust stance and to have a well distributed leg contact area. The effectiveness of the C-leg in the hoop orientation can be seen in RHex's ability to run in complex terrain [14].

### Design

#### Design of Spines

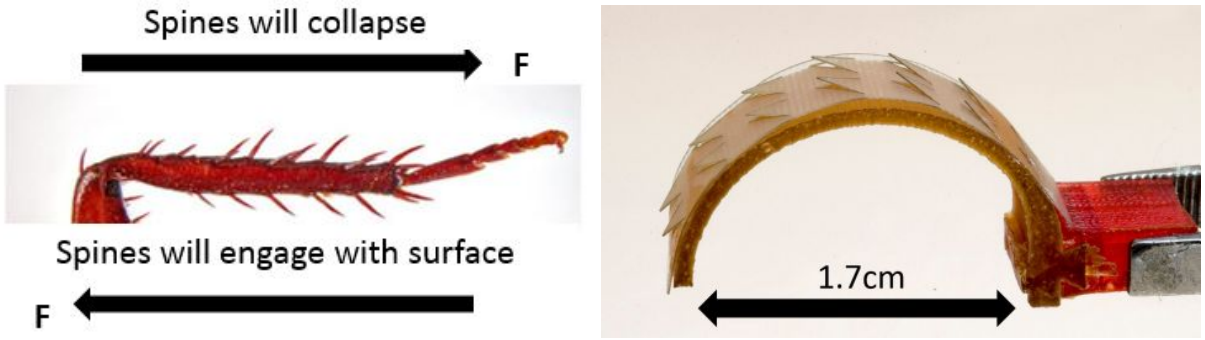


Figure 2.2: (Left) Anisotropic properties of cockroach leg spines. (Right) Spines attached to a leg.

The anisotropic collapsible spines shown in Fig. 2.2 are inspired by the passive leg spines on cockroach's tibia-tarsus joint. They enable cockroaches to run on horizontal, rough terrain and compensate for the absence of feet on steep inclines [23]. Their anisotropy allows them to collapse when pushed in one direction, but engage and stop at a certain angle when pushed the other way. To mimic this architectural advantage, the spines are fabricated from 0.125 mm thick fiberglass with an array of 45° wedges cut out that measure 2.54 mm x 2.54 mm. The uncut fiberglass conforms to the C-leg, causing the released triangles to stick out of the leg. The triangles are also skewed such that only one edge is parallel to the edge of the leg,

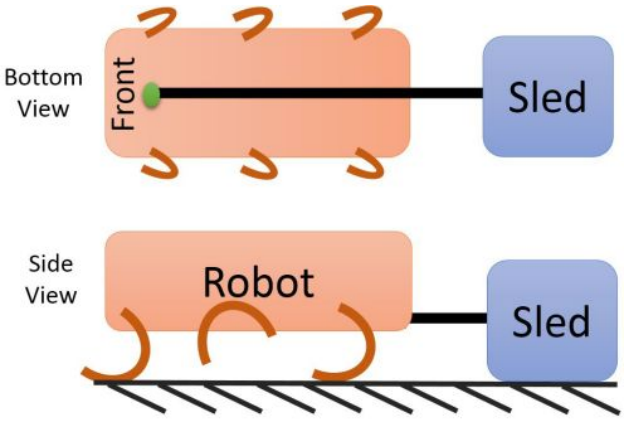


Figure 2.3: Diagram of the robot pulling a load on a sled. On the top is a bottom view of the VelociRoACH showing the attachment at the front of the belly. On the bottom is a side view of the robot pulling a sled.

while the other is skewed to give it lateral as well as fore-aft anisotropy. For more details on manufacturing process of the spines refer to [18]. While the spines are intended to give the leg better traction by catching on asperities in the surface, they also change the compliance of the leg with the addition of fiberglass. To minimize the effects of stiffer legs, we ran the robot at relatively slow speeds during our experiments.

#### Sled Design

The thrust performance of a VelociRoACH with spines was measured by loading weights into an attached sled (Fig. 2.3). The sled was a plastic container with an open top for easy access to load weights. A plastic sheet of Stretchlon[1] was hot glued to the underside of the sled. The coefficient of static friction (0.45) was found by analyzing a force balance at the moment of slip on an inclined plane, while the dynamic friction coefficient ($\approx 0.4$) was found at the incline where it stopped slipping. A string was then glued around the outside of the sled and attached to the underside of the VelociRoACH in front of its center of mass to prevent it from pitching upwards while running.

## 2.3 Results

### Performance of Leg Spines

Load-drag-pull tests [15] were performed on corkboard with a single robot leg in the fore-aft and lateral directions using a 3 axis linear stage that moved over a force sensor (Fig. 2.4

[1] from Fibre Glast

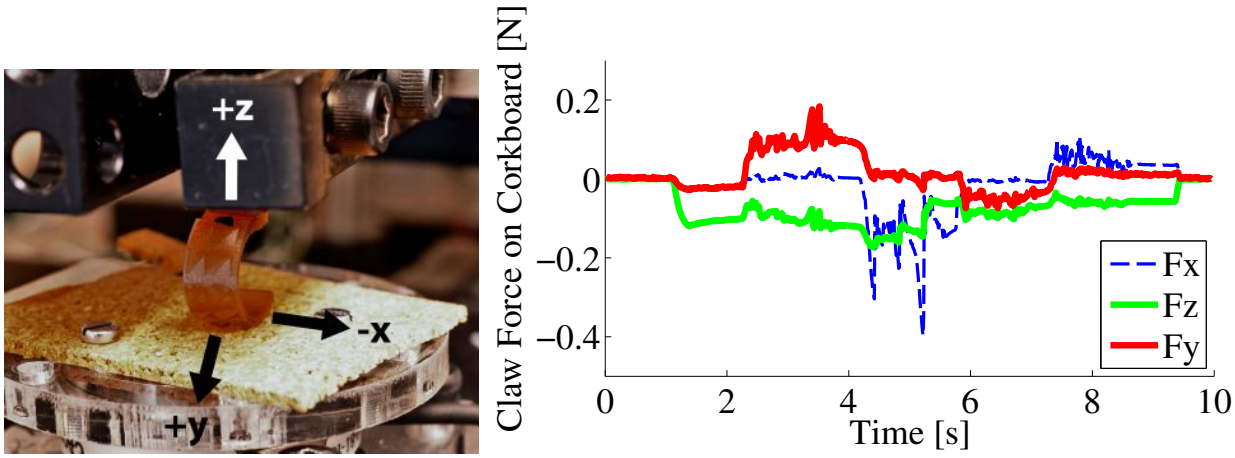


Figure 2.4: (Left) Leg with spines during a load-drag-pull test on a force-torque sensor covered with cork board. (Right) Plot of forces during a load-drag-pull test of a foot with spines on corkboard. The leg was pre-loaded in the -z direction, then dragged in a square formation in the following directions: $+y$, $-x$, $-y$, and then $+x$.

left). For an extended description of this test performed with a leg with spines on cloth refer to [18]. Corkboard was used for all the following experiments because it is a simple first material for spine engagement. The recorded force profile for a representative trial shows the normal loading force $F_z$, the fore-aft force $F_y$, and the lateral force $F_x$ (Fig. 2.4 right). While the spines are penetrating the surface, the force limit of the foot is 0.197 N. The force limit in the opposite direction to make the spines collapse is 0.104 N, for a 2:1 ratio between the force limits for spine engagement and slip (Fig. 2.5).

In lateral testing, more force was required to disengage the foot in the direction of the triangle edge parallel to the foot edge than in the direction of the skewed edge. In comparison, the foot without spines has the same force limits in both lateral directions and a very low holding force in the positive $y$ direction (Fig. 2.5). Although the spines seem to provide a greater holding force in the lateral direction, we chose to utilize the spines so that the point of the triangle engages the surface to better catch onto asperities. Additionally, in its current configuration the spines function similar to a cantilever beam where the root of the beam starts at the leg surface and the leg curves away. If we turn the triangles sideways, the cantilever beam will no longer be in the direction of the curve and the leg will no longer curve away from the beam. This would make manufacturing more difficult since the spines won't stick out naturally. It should be noted that the high release force in the leg without spines in the positive $y$ direction was due to buckling in the leg during the load-drag-pull test, which happened when the leg tip engaged the ground. Buckling did not occur in the legs with spines because they were less compliant. The buckling behavior can be further explained by a pseudo-rigid body model of an initially curved, end-force loaded cantilever beam [21].

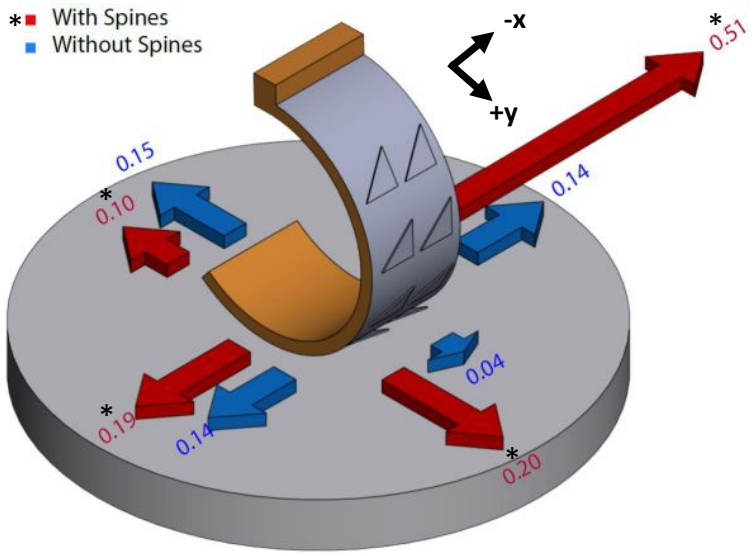


Figure 2.5: The maximum force limits in Newtons of the leg with and without spines on corkboard. Arrows indicate the direction of the force and the number indicates the average force.

From these tests we can see that to disengage the spines we could either slide the leg forward, making the spines collapse, or pull the leg sideways toward the skewed edge of the triangle. With these results we can also find the coefficient of friction of the foot with and without spines by dividing the drag force by the normal force. In the positive $y$ direction, a leg with spines has a friction coefficient of $1.04 \pm 0.19$ while without spines it has a friction coefficient of $0.18 \pm 0.04$.

## VelociRoACH Free Running and Slope Traversal

To evaluate the spine's utility on a robotic platform, running tests were conducted using a VelociRoACH on corkboard (Fig. 2.7 left). For these free running tests the robot ran on a surface where the incline was easily adjustable and the robot's stride frequency was controlled.

### Speed on Flat Ground and an Incline

In the first set of tests, the robot was run at various stride frequencies on flat ground and at a 20° incline (Fig. 2.6). Speed was obtained using distance and running time recorded. The average speed of a robot running on flat ground at 5 Hz with spines and without spines was 0.18 m/s and 0.13 m/s respectively. On a 20° incline, the average speed of a robot with spines and without spines was 0.13 m/s and 0.03 m/s respectively. After performing an Analysis

of Variance (ANOVA) test, all speeds taken from a robot with spines were determined to be significantly faster than the speeds of a robot without spines.

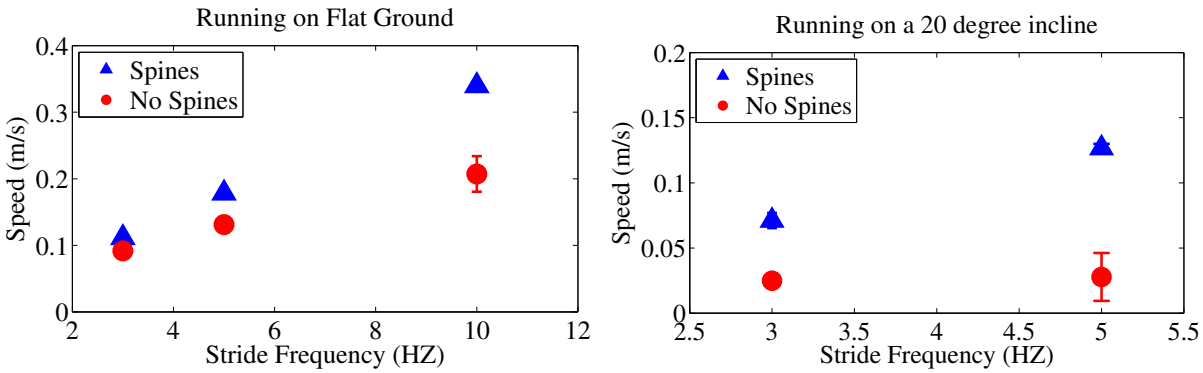


Figure 2.6: All tests were performed with the same robot and each trial was tested three times. (Left) The speed of a VelociRoACH with and without spines running at various stride frequencies on flat ground. (Right) The speed of a VelociRoACH with and without spines running at various stride frequencies on on a 20° incline.

### Maximum Incline

In order to find the maximum incline the robot could run, the robot was set at a specific stride frequency and the incline was slowly increased until the robot could not progress in the forward direction. From Fig. 2.7, we see that at 3 Hz the maximum incline for a robot with and without spines was 34° and 27° respectively. According to an ANOVA test, the robot with spines was able to run up significantly higher inclines.

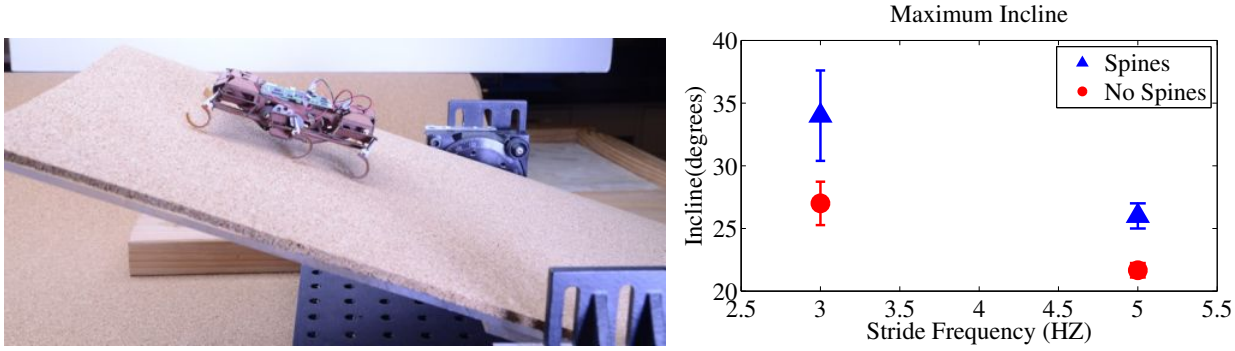


Figure 2.7: (Left) VelociRoACH running up an incline covered in corkboard. (Right) The maximum incline of a VelociRoACH with and without spines. All tests were performed with the same robot and each trial was tested three times.

## VelociRoACH Pulling a Load

To evaluate the spine's utility during advanced tasks, pulling tests were conducted using a VelociRoACH on corkboard (Fig. 2.8). It is known from biology that pulling is significantly more energetically expensive [12], so pulling tests are a good way to quantify whether spines improve robot performance in difficult tasks. Pulling is also a better experiment to measure energy expenditure than carrying because carrying would alter the normal force of the robot. This in turn would affect the friction coefficient of the spines.

### Cost of Pulling

In the first set of tests, the robot had a constant towing load of 0.2 N while the stride frequency was incrementally increased. In the next set of tests, the robot was run at a constant 3 Hz stride frequency while the pulling force of the sled was increased incrementally by putting different weights in the sled. Distance traveled and the electrical power drawn by the motors were recorded in order to find the speed of the robot and the Cost of Pulling (CoP), Eqn. (2.1). Useful work was calculated using the measured coefficient of friction of the sled (0.4), the weight of the sled, and the distance the sled moved. The CoP was found by dividing the energy used by the motors by the useful work of the sled being pulled(Eqn. 2.1). I used CoP as opposed to Cost of Transport (CoT) because CoT only takes into account the robot's weight, and I wanted to capture the additional effort required to pull added weight.

$$CoP = \frac{Power \cdot Time}{Force \cdot Distance} \tag{2.1}$$

For a constant pulling force, CoP in the VelociRoACH decreases as the stride frequency increases and the VelociRoACH with spines always has a lower CoP (Fig. 2.9 left). At a stride frequency of 5 Hz, the CoP of the VelociRoACH without spines has a value of 3700 while the value with spines is 330, showing a decrease of about 10 times.

For a constant stride frequency at any amount of pulling force, the VelociRoACH with

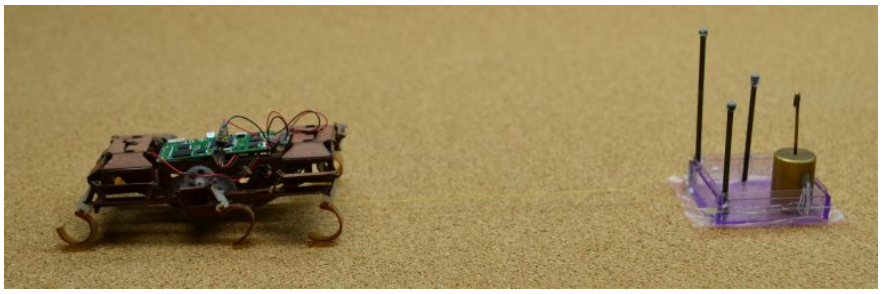

Figure 2.8: Sled with a weight in it being pulled by a VelociRoACH with spines on corkboard.

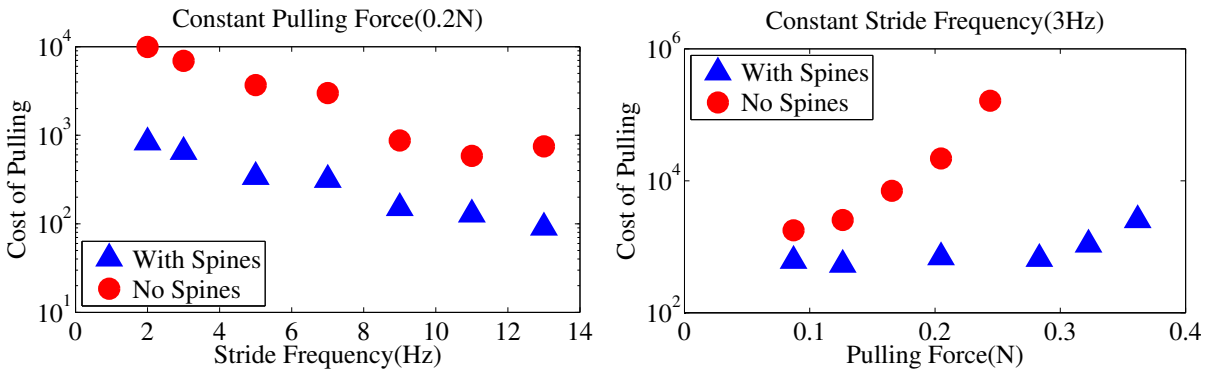


Figure 2.9: All tests were performed with the same robot and each trial was tested three times.(Left) The Cost of Pulling for a VelociRoACH with and without spines at a constant pulling force using various stride frequencies. (Right)The Cost of Pulling of a VelociRoACH with and without spines using various pulling forces at 3 Hz.

spines has a lower CoP than without spines and the CoP increases as the pulling force increases (Fig. 2.9 right). It should be noted that the robot without spines could not pull more than 0.25N, and would slip in place. At a pulling force of 0.2 N, the CoP of a VelociRoACH with spines has a value of 700, whereas without spines the value is 2200, showing about 30 times the increase. This implies that for a certain amount of energy input, the robot could do more useful work simply by adding spines when moving on a material such as corkboard. For example, a VelociRoACH without spines expends 4.2 W of power to tow 0.09 N forward, whereas a VelociRoACH with spines using 4.3 W can pull 0.28 N. Therefore with almost the same amount of power, a robot with spines can pull more than three times the amount it could pull without spines. This is also the equivalent of pulling a broken or unused VelociRoACH in a sled (0.12 N), increasing the number of deployments. Additionally, this improvement of CoP could increase the range for each robot, which is critical in search and rescue missions.

### Speed Enhancement while Pulling

Speed was obtained by using the distance and running time recorded during our pulling tests. For constant stride frequency, the speed of a VelociRoACH with spines was significantly greater at all tested loading forces (Fig. 2.10 left). The VelociRoACH without spines starts slipping at 0.2 N of pulling force, whereas with spines it can pull up to 0.36 N. During the constant pulling force tests the VelociRoACH with spines was still able to move faster than the case without spines (Fig. 2.10 right). Without spines at high frequencies, however, the VelociRoACH was not moving forward even though its legs were still moving rapidly. This implies that the pulling force is exceeding the VelociRoACH's leg friction force limit, which is the product of coefficient of kinetic friction and normal force. The VelociRoACH with spines, on the other hand, engages the surface but is unable to move its legs with a 0.36 N pulling load. Therefore the robot is friction limited without spines and torque limited with spines.

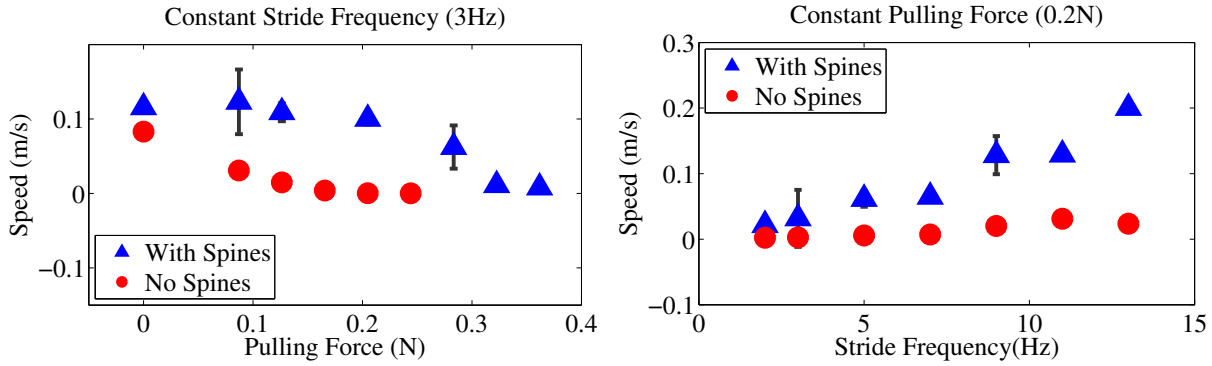


Figure 2.10: All tests were performed with the same robot and each trial was tested three times. (Left) Speed of sled while the VelociRoACH pulled various forces at a constant stride frequency of 3 Hz with and without spines. (Right) Speed of the sled at various stride frequencies while the VelociRoACH had a constant induced pulling force of 0.2N with and without spines.

To examine more closely whether the robot is now torque limited, graphs of the motor torque are shown in Fig. 2.11 (motor torque is estimated from motor current and torque constant). The bottom row represents the motor torque when the robot is pulling the largest force it can, 0.2 N for a robot without spines and 0.36 N for a robot with spines. In the left plots of Fig. 2.11, the blue solid line represents the motor torque of the VelociRoACH without spines and the red dashed line represents the theoretical torque at which the foot will slip (0.8 mN-m), taking into account the coefficient of friction from the load-drag-pull tests. The motor torque is consistent for all pulling loads and reaches a maximum of 1 mN-m, which is close to the value where the foot will slip. In the graphs of the motor torque of a robot with spines (Fig.2.11 right), the red dashed line represents the maximum torque the motor can produce (1.6 mN-m). While pulling 0.1 N the motor torque reaches 1.4 mN-m, which is close to the maximum value for the maximum motor torque, and at 0.36 N the motor stalls.

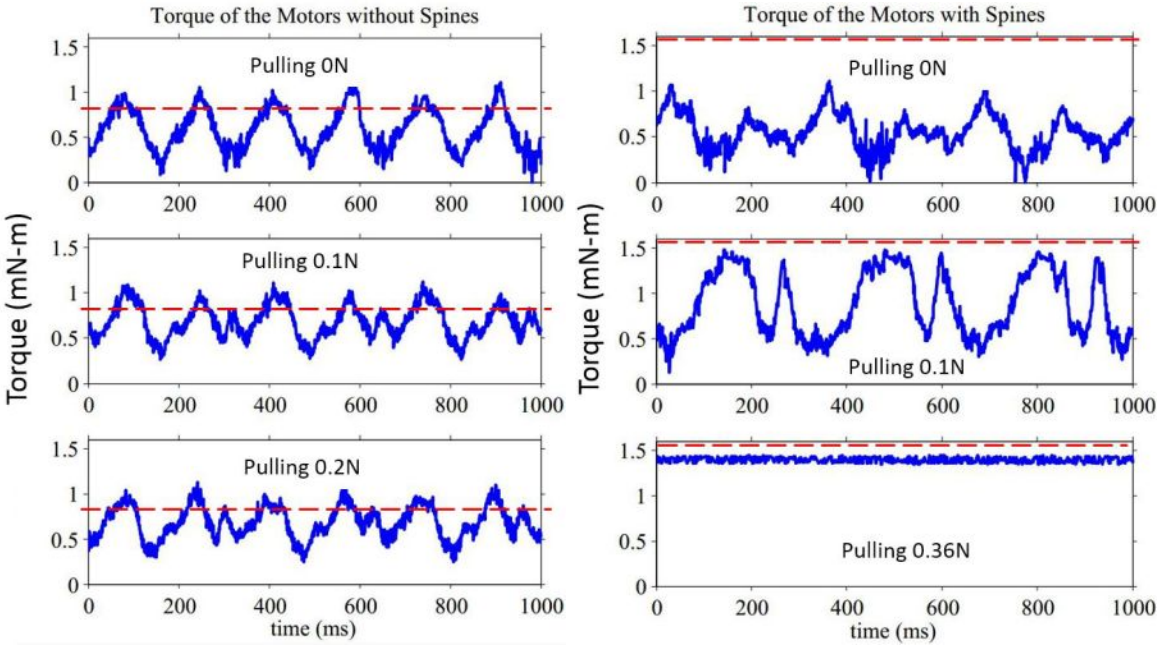


Figure 2.11: (Left) Motor Torque of the VelociRoACH without spines taken over 3 cycles with a pulling force of 0N, 0.1N and 0.2N. Red dashed line indicates the torque at which the feet will theoretically slip. (Right) Motor Torque of the VelociRoACH with spines taken over 3 cycles with a pulling force of 0N, 0.1N and 0.36N. Red dashed line indicates the maximum torque of the motor used in the robot.

### Resistance to Torque Disturbance

To examine the robot's heading behavior while pulling a load, the sled was attached in the center of the robot while an OptiTrack system tracked the sled and Matlab was used to plot its path. A pulling force of 0.1 N was used while the robot ran over corkboard because this was a configuration easily managed by the VelociRoACH with and without spines. The trajectory of the sled appears fairly straight in Fig. 2.12 when the sled was attached to the center of the robot. Therefore the robot with and without spines is dynamically stable and can maintain a straight heading.

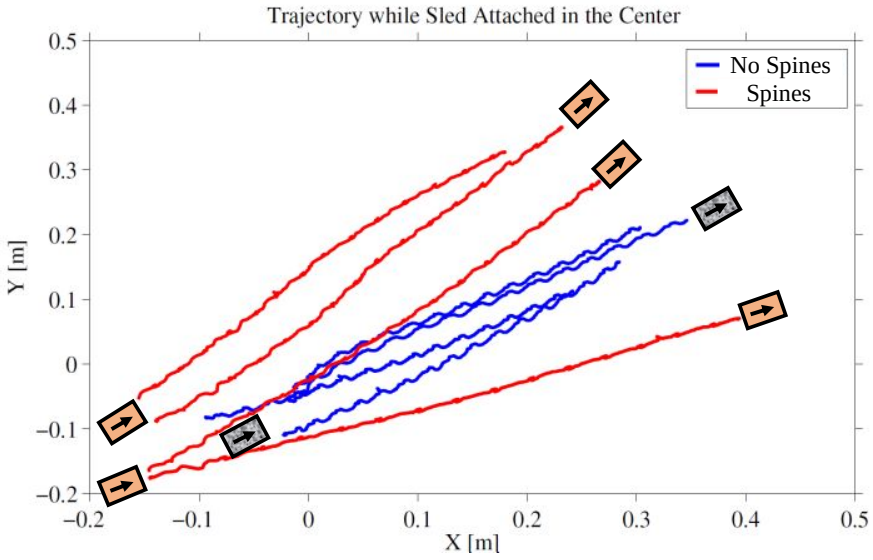


Figure 2.12: Trajectory of the VelociRoACH with and without spines while pulling a sled attached to the front, center belly of the robot. Boxes indicate the sled's position while arrows indicate the direction the robot is facing. The orange boxes are the sled pulled by robot with spines, and the grey speckled boxes are pulled by the robot without spines. The trajectory for both cases of the VelociRoACH with and without spines seem fairly straight.

Next a deliberate yaw torque bias was applied to examine the effect on heading behavior. To induce an initial moment, the sled was attached to alternate sides on a carbon fiber rod with bumps spaced 1 cm apart to hold the sled (Fig. 2.13). By controlling the lateral offset of the sled from the body, the magnitude of the torque disturbance could be tuned to create a noticeable turn in either direction.

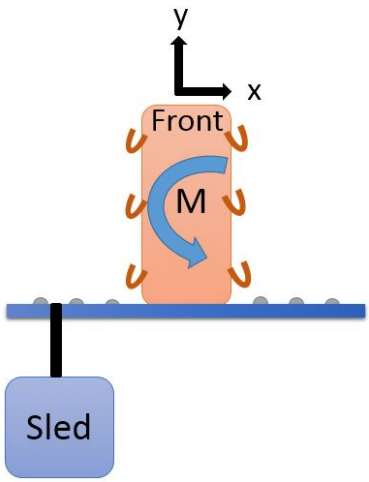


Figure 2.13: Top view of the robot with the sled attached to a rod on its back.

For the right side an induced moment of 4 mN-m was required to produce a significant right turn for a robot without spines. However on the left side, due to asymmetries in the robot, the VelociRoACH without spines required a 6mN-m moment to produce a left turn of similar magnitude. It should be noted that because the moment is induced by a sled attached by a freely rotating string, the true moment to induce yaw shown by Fig. 2.13 is only applied at the first instant. Once the robot begins to turn, the tension force on the robot will be in a different direction.

From the tracked sled trajectory (Fig. 2.14), the VelociRoACH with spines seems to show greater resistance to torque disturbance as it tries to run towards positive $y$. Overall it follows the original heading farther than the robot without spines. Similar to the model of a passive dynamic self-stabilizing system of cockroaches by Full *et al*. 2002 [13], the robot with spines seems to be neutrally stable by following a certain trajectory after being perturbed and not returning to its original path. Interestingly, there are even a few runs in Fig. 2.14 where the robot veers toward the opposite direction that is predicted. For example, the robot runs to the right even though the sled is attached to its left. This could be caused by tension from the sled giving the left feet more traction, over powering the right side and causing the robot to go right. However further work will be needed to confirm this hypothesis.

## 2.4 Conclusions

The bio-inspired spines evaluated in this paper give the VelociRoACH a variety of performance advancements from a simple leg enhancement. The increase in foot friction has increased the maximum incline the robot can traverse by ten degrees. The speed of the VelociRoACH with spines is significantly higher than a robot without spines, regardless of the pulling force, stride frequency, or incline. Additionally, the Cost of Pulling in the Ve-

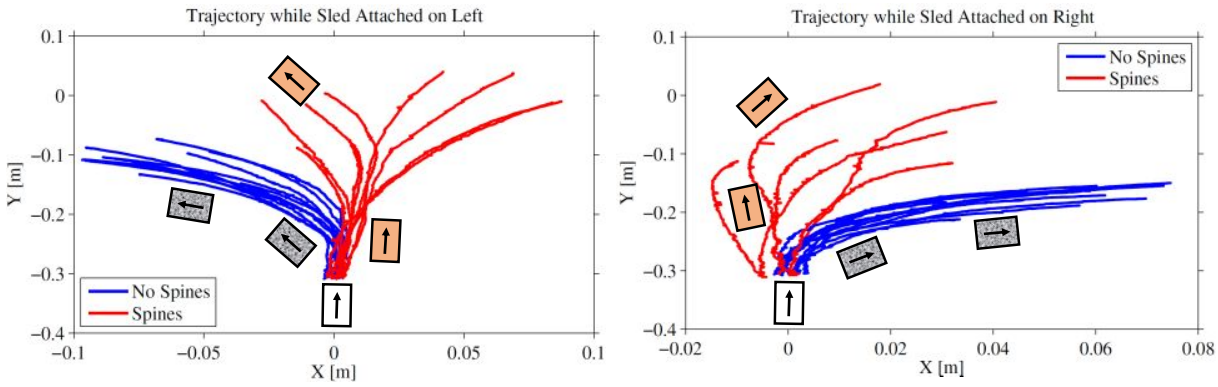


Figure 2.14: Boxes indicate the sled's position while arrows indicate the direction the robot is facing. The white box is the starting position of the sled pulled by the robot with or without spines, the orange boxes are the sled pulled by the robot with spines, and the grey speckled boxes are pulled by the robot without spines.(Left) Trajectory of the sled being pulled by a VelociRoACH with and without spines with a 6mN-m initial torque. (Right) Trajectory of the sled being pulled by a VelociRoACH with and without spines with a 4mN-m initial torque.

lociRoACH has decreased by an order of magnitude when pulling a significant load force, which has increased its towing capacity per unit energy. This is useful in the world of small robotics where weight and body real estate is critical. Although towing is an energetically expensive task, this could be used for short periods of time when other robots need assistance relocating or for transporting equipment. The spines also stop the robot from slipping and allow it to pull 0.16 N more than without spines, making the VelociRoACH torque limited instead of friction limited on corkboard. Finally, the VelociRoACH with spines resists torque disturbances better and is neutrally stable. All these improvements make the VelociRoACH a more useful robot for applications such as search and rescue, where the robot will have to navigate challenging terrain and possibly pull payloads.

# Part II

# Insights from Biology

# Chapter 3

# Crickets using Spines to Jump

## 3.1 Introduction

Insect legs possess various structures that can enhance interaction with the substrate. From an engineer's point of view, it is fascinating with the way animals are able to engage with and navigate through their environment successfully. A critical aspect of this is traction through interlocking. To gain insight on spines, I researched how crickets use spines on their tibia to jump on different substrates (Fig. 3.1).

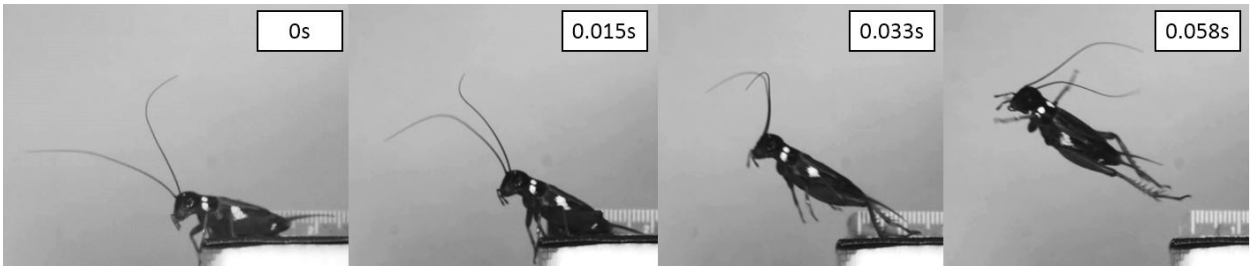


Figure 3.1: Cricket jumping off of sandpaper.

## 3.2 Methods

*Gryllus firmus* were used in the experiments, which are field crickets that are about 2 cm long. There were three different foot configurations to isolate and test the spines on their tibia, shown in Fig. 3.2. First they were jumped on different surfaces completely intact, which is the control case. This allows them to use both the tibia spines and attachment pads on the tarsi. Next their tarsi was glued up, which took away their attachment pads and isolated the spines. In the last set of experiments, the spines were trimmed and super glue was applied over the end of the tibia. In this case the crickets did not have the use of

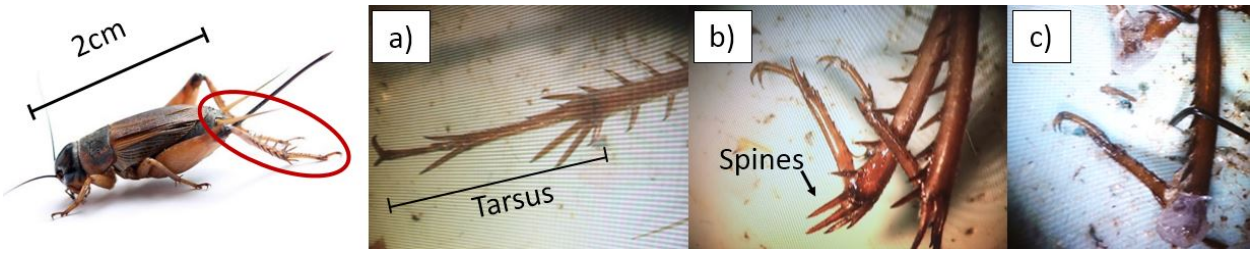


Figure 3.2: Different foot configurations. a) Cricket has use of tibia spines and tarsi attachment pads. b) Cricket can only use spines. c) Cricket has no spines or attachment pads.

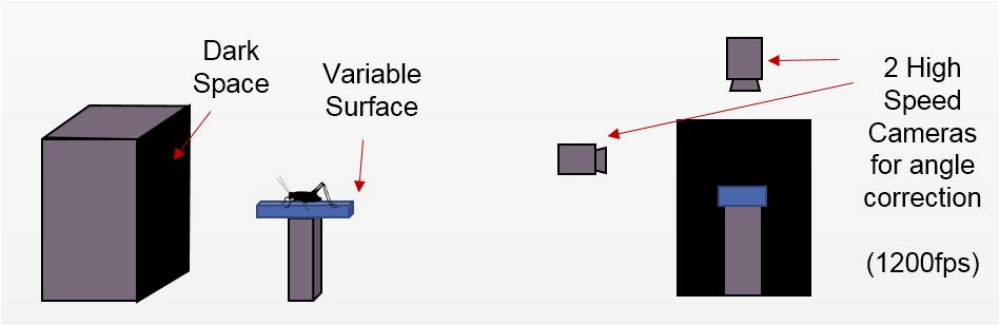


Figure 3.3: Test set up for cricket jumping.(Left) Side view showing where the cricket jumps from. (Right) Back view showing where the cameras are in relation to the cricket stand.

either attachment pads or spines. There were four different surfaces: glass, sandpaper, sand, and styrofoam. There were eight individuals, and four trials were run for every combination of individual, foot configuration, and surface type.

Fig. 3.3 shows the test set up where the cricket jumps off an elevated platform with an interchangeable surface towards a dark space. High speed cameras were used at 1200fps with a small field of view to film the instantaneous take off velocity. Crickets were filmed from the top and side to correct the velocity if the animal jumped out of plane. This resultant velocity was used to find kinetic energy, which is how each animal's jumping performance was measured. Modified load-drag-pull tests were also performed from Fig. 2.4 (left) to include a cricket leg over the force sensor covered with Styrofoam. For a more detailed description of the test, refer to Chapter 2. The leg was moved in both the positive $y$ and negative $y$ directions. Positive $y$ drags the leg over the force sensor in the direction of its body, so that the spines can collapse. The negative $y$ direction drags the leg in the direction of the end of the tarsi, where the spines are allowed to engage with the substrate.

Table 3.1: Friction Coefficient of Cricket Leg

| Friction Coefficient Direction | Spines and Pads | Spines | No Spines or Pads |
|---|---|---|---|
| Positive Y | 0.41±0.02 | 1.42±0.87 | 3.11±0.61 |
| Negative Y | 3.04±0.50 | 3.24±0.29 | 2.73±1.01 |

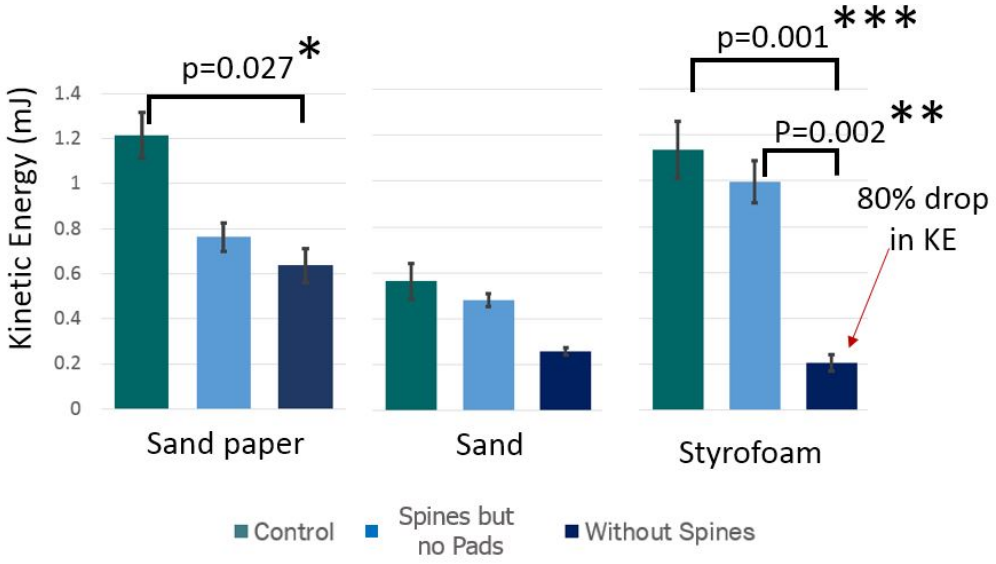


Figure 3.4: Kinetic energy of crickets jumping on sandpaper, sand, and Styrofoam.

## 3.3 Results

Table 3.1 shows the results of the load-drag-pull tests. For both the case with spines and spines with attachment pad, there is more friction in the negative $y$ than positive $y$ direction, indicating that the foot structures provide the leg with more traction.

Fig. 3.4 shows the kinetic energy at launch as it varies with foot configuration on the sandpaper, sand and Styrofoam. Glass results are not shown because crickets slipped and could not jump on the glass. I performed these experiments with the control case (in green), just spines but without attachment pads (light blue), and without spines and attachment pads (dark blue). After doing a statistical analysis in R, there were no individual effects. Note that for the control case, the kinetic energy jumping on sand is 53% lower than sandpaper, whereas the Styrofoam yielded similar performance. Disabling their tarsi, and therefore the attachment pads they have, had no significant effect on jumping from these substrates. However, removing spines had a large effect on the high traction surface and penetrable substrate. On the penetrable substrate there is an 80% drop in performance from having spines to not having spines, therefore spines significantly increase kinetic energy on a surface that's easy to penetrate.


Figure 3.5: a) An unaltered grasshopper leg showing the attachment pads and spines. b) After gluing up the tarsi, the spines are still able to be used. c) The spines are trimmed and glued.

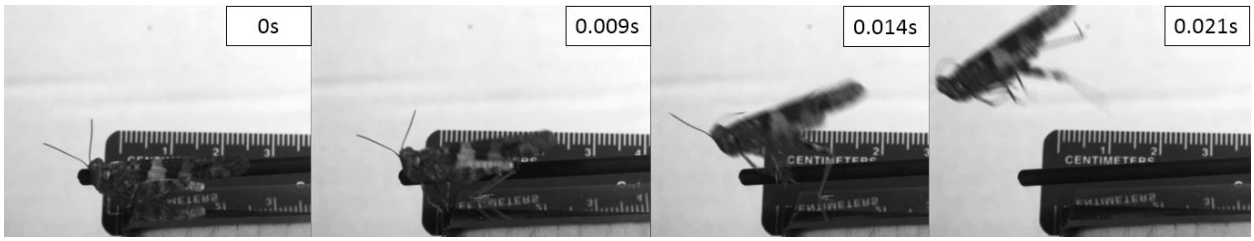


Figure 3.6: Grasshopper jumping off of glass.

## 3.4 Grasshopper Preliminary work

I was only able to obtain two live grasshoppers (*Trimerotropis pallidipennis*), so these are just preliminary experiments. The grasshoppers had a more pronounced attachment pad, shown in Fig. 3.5. This seemed to help them jump on smooth surfaces, as they were able to jump on glass while crickets cannot. However, they also had a different jumping strategy and seemed to launch their center of mass upwards instead of jumping head-first in a forward direction (Fig. 3.6). This jumping direction also propelled them towards the lights, instead of the dark box. This strategy allowed them to use their jumps for takeoff, and they always unfurled their wings and flew soon after jumping.

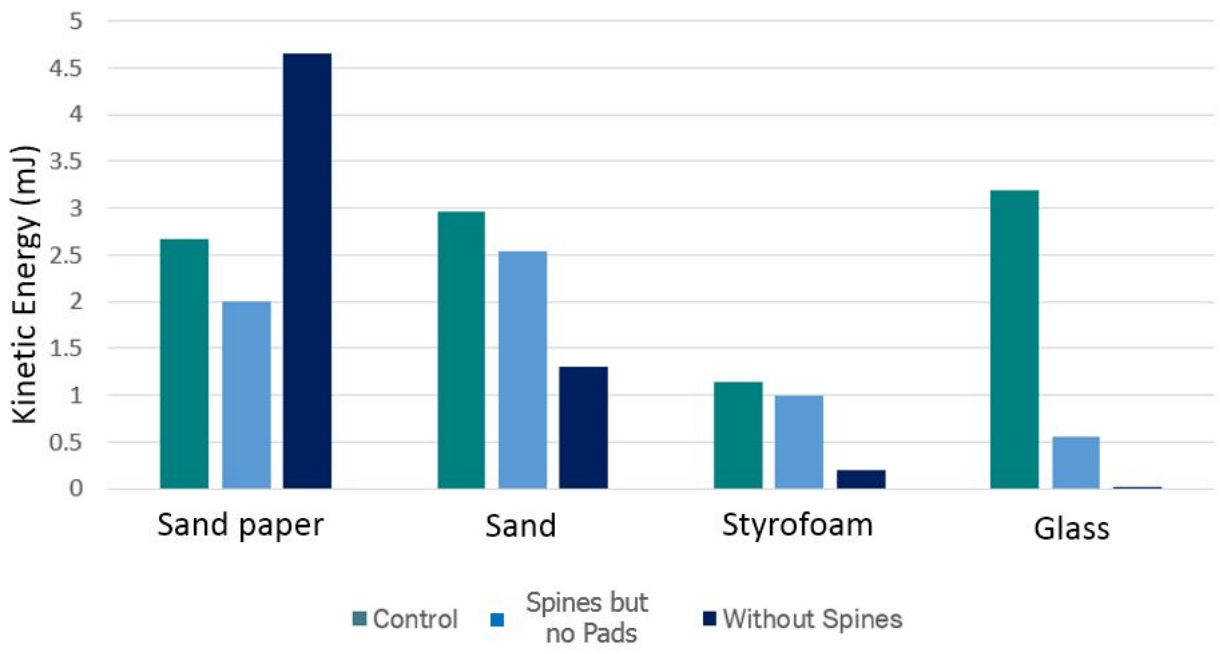


Figure 3.7: Kinetic energy of grasshoppers jumping on sandpaper, sand, Styrofoam, and glass

### Results

Fig. 3.7 shows the kinetic energy of the grasshoppers jumping with different foot configurations on sandpaper, sand, Styrofoam, and glass. For the control case, grasshoppers seemed to have the lowest performance on Styrofoam. When the attachment pads were removed, the performance on glass dropped by 82% . When the spines were removed, the performance dropped by 50% on sand and 80% on Styrofoam. There was an increase in performance on sandpaper, but more trials and individuals are needed to explore this, since only one individual was available to test without spines and attachment pads on sandpaper.

## 3.5 Conclusion

For crickets there was no change in kinetic energy on glass and sand, but a small change on sandpaper and a large increase on Styrofoam with spines. For grasshoppers there was also an increase in performance on Styrofoam with spines, as well as sand. Preliminary grasshopper tests also showed that attachment pads increase performance on glass. Therefore, spines seem to be useful on penetrable surfaces, whereas attachment pads are used for smooth hard surfaces.

# Part III

# Bio-inspired Spines for Jumping in Robots

# Chapter 4

# Compound Foot for Increased Millirobot Jumping Ability

## 4.1 Introduction

Jumping robots are useful for search and rescue applications because they are able to navigate obstacles many times their body height. However, to reach a certain destination and travel in the horizontal direction, robots need traction. Taking what I found from the cricket experiments, I created bio-inspired compound feet to increase the horizontal jumping performance of a 2g jumping robot. Compliant leg spines provide distributed mechanical feedback, while sticky attachment pads allow insects to traverse vertical and inverted smooth surfaces [11]. Unlike past examples, the designs presented in this work are the first studies on the novel application of spine traction to millirobot jumping.

## 4.2 Design

### Robot Platform and Modeling

The robot used in this work was developed in the BioRobotics Lab at Seoul National University. It is 2cm long, and can jump 30 times its body size [35]. This robot utilizes a four-bar mechanism to simulate a flea's leg kinematics and is constructed using the Smart Composite Microstructures Process (SCM) [49]. Shape memory alloy (SMA) spring actuators were used for a bio-inspired catapult system that quickly releases energy by torque reversal triggering.

This robot was specifically chosen to use spines because of its leg mechanics, reaction force pattern, and size (Fig. 4.1a). Unlike many other jumping robots, the legs rotate outward and push off the ground in the horizontal direction, which the spines need for engagement. This was confirmed with the model used in the original robot experiments [35]. This Matlab model was used to find the best case by deliberately simulating no-slip conditions. (For the kinematics and equations governing the dynamics of the robot during flight, please refer

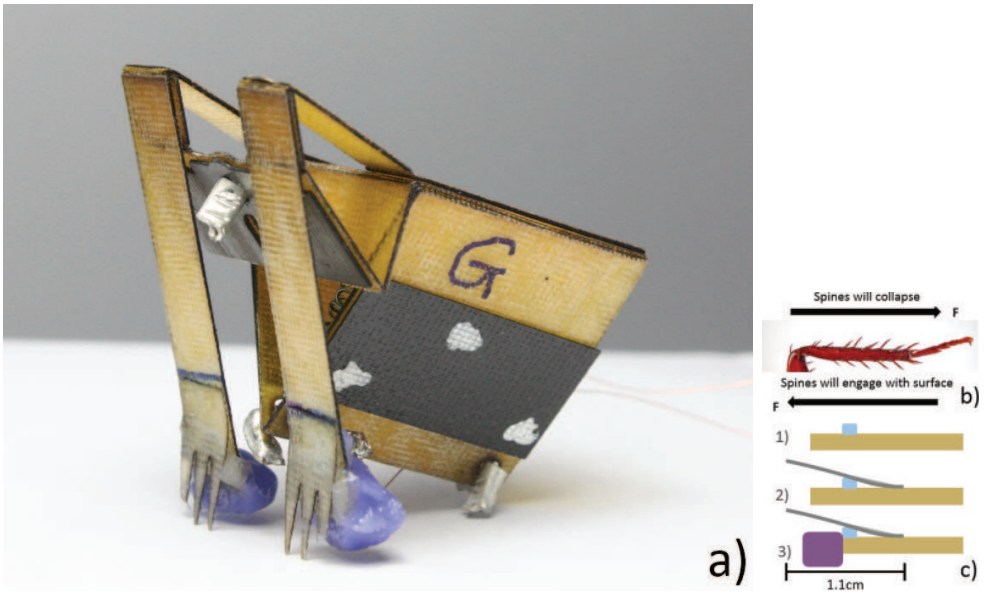


Figure 4.1: a) Flea robot with compound feet that include spines and attachment pads. b) Anisotropic properties of cockroach leg spines. c) The manufacturing process for attaching the spine and attachment pad.

to [35]) The geometric dimensions, spring stiffness of the extensor muscle, and mass in the model were changed to match the current robot with spines attached. The model showed that angling the body forward created a larger and earlier horizontal force approximately proportional to the vertical force (Fig. 4.2). Fig. 4.2a-d shows the progression of the jump, where the leg first engages the surface, engages without slipping, and then propels the robot forward and upwards.

## Insect Inspired Spines and Attachment Pad

The spines on the robot feet shown in Fig. 4.1a are inspired by the passive leg spines on cockroaches tibia-tarsus joint (Fig. 4.1b). These spines are similar to ones used by crickets during jumping [30]. To mimic this passive surface engagement mechanism, the spine attachment is fabricated from a 6mm x 11mm piece of 6 ply, 0.12 mm thick fiberglass with 3 points cut out. These spines increase the weight of the robot by 2.5%. To attach the spines, a 2mm thick piece of super soft silicone (Ecoflex 30 by Smooth-On) is placed on the leg (shown in part one in Fig. 4.1c). The spine is glued onto the leg over the silicone, causing it to stick out of the leg at 20° to more directly engage surface asperities.

The attachment pad, shown in Fig. 4.1a and part three in Fig. 4.1c, is based off of the insect attachment pads observed on the grasshopper to prevent slip on smooth surfaces [30]. The leg under the spine is dipped in a mix of resin and hardener several times until the

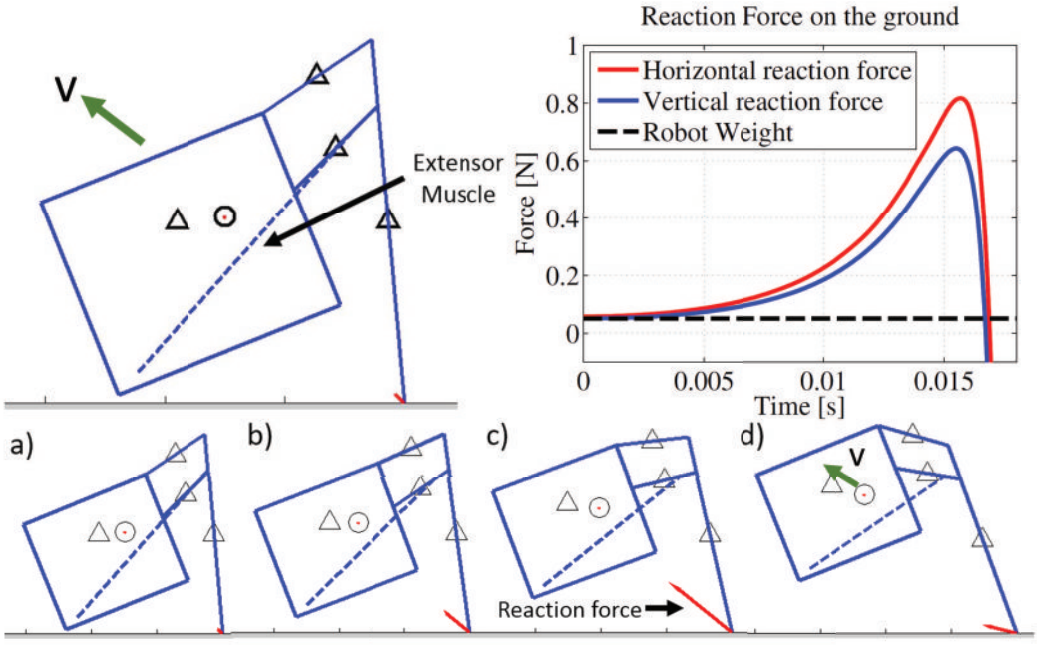


Figure 4.2: (Top Left) The no-slip model of the robot in Matlab with a spring as the extensor muscle. The model represents the robot just after triggering, where the extensor muscle has lowered past the bottom leg joint. (Top Right) Plot of the horizontal and vertical reaction forces as the robot in the Matlab model jumps with no-slip conditions. (Bottom) Sequential pictures of the Matlab model of the robot jumping with no-slip condition. Frame d is just before take off.

desired attachment pad height is achieved, such that if the spine slips and the leg rotates, the attachment pad will engage the surface. Here the attachment pads are 4mm tall and add 0.14g of weight, increasing the robot mass by 6%.

## 4.3 Results

### Performance of Leg Spines

Vertical compression tests were performed on a single robot leg using a force sensor and sandpaper to prevent slipping (Fig. 4.3). The surface first moved into the spine to create a preload and bend the spines inward to mimic a normal jump (Fig. 4.5d). This buckling gives the spine higher friction than if the spines were bent in the other direction, and can be further explained by a pseudo-rigid body model of an initially curved, end-force loaded cantilever beam [21]. Using the spine compression and force measured from these tests,

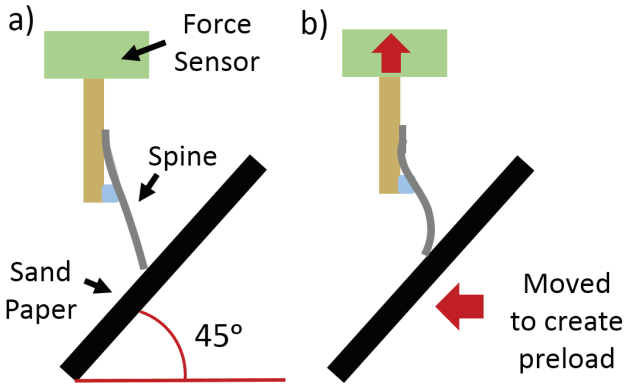


Figure 4.3: Leg with spine during a stiffness test using a 1 axis force sensor and sandpaper as the engagement surface.

the spine stiffness was determined to be 2.4±0.1 kN/m. This value was used in the no-slip model.

## Jumping Performance of Robot With and Without Spines

To evaluate the spine's utility during jumping on a robotic platform, the robot was tested on three different surfaces: Teflon, Styrofoam, and silicon carbide sandpaper of grit size 60. Three trials were recorded with a video camera to view the overall jump and a high speed camera with a small field of view to capture the take off velocity. The robot was tested first without spines, then with spines, and later with attachment pads. The robot without attachment pads was unable to jump on Teflon, but could jump on both Styrofoam and sandpaper. The jump trajectories of a robot with and without spines can be seen in Fig. 4.4. The jump of a robot without spines can be seen in Fig. 4.5, where one leg slips at moment Fig. 4.5b. However, with spines the robot is able to engage the surface and the spines bend at instant shown in Fig. 4.5d as the leg rotates out.

To compare the robot performance on different surfaces we calculated kinetic energy and take off angle, since they directly affect parameters such as the horizontal distance the robot can travel. Kinetic energy was calculated using take off velocity, and take off angle was tracked from video footage. The take off angles in all trials ranged from 32°- 37° and were statistically insignificant from each other from an ANOVA test. Therefore in this chapter we will be focusing on the kinetic energy results shown in Table 4.1.

On sandpaper, a surface with reasonable engagement for an unaltered robot, the kinetic energies for the robot with and without spines are close to the no-slip model's values of 6.6mJ. The spines decreased the rotational velocity by 8% and the kinetic energy in the robot experiment from 6.4mJ to 5.8mJ (Table 4.1), however these values are not statistically different from each other. On Styrofoam the robot without spines slips. The spines increase the kinetic energy from 3.6mJ to 6.0mJ which is a statistically significant increase, bringing

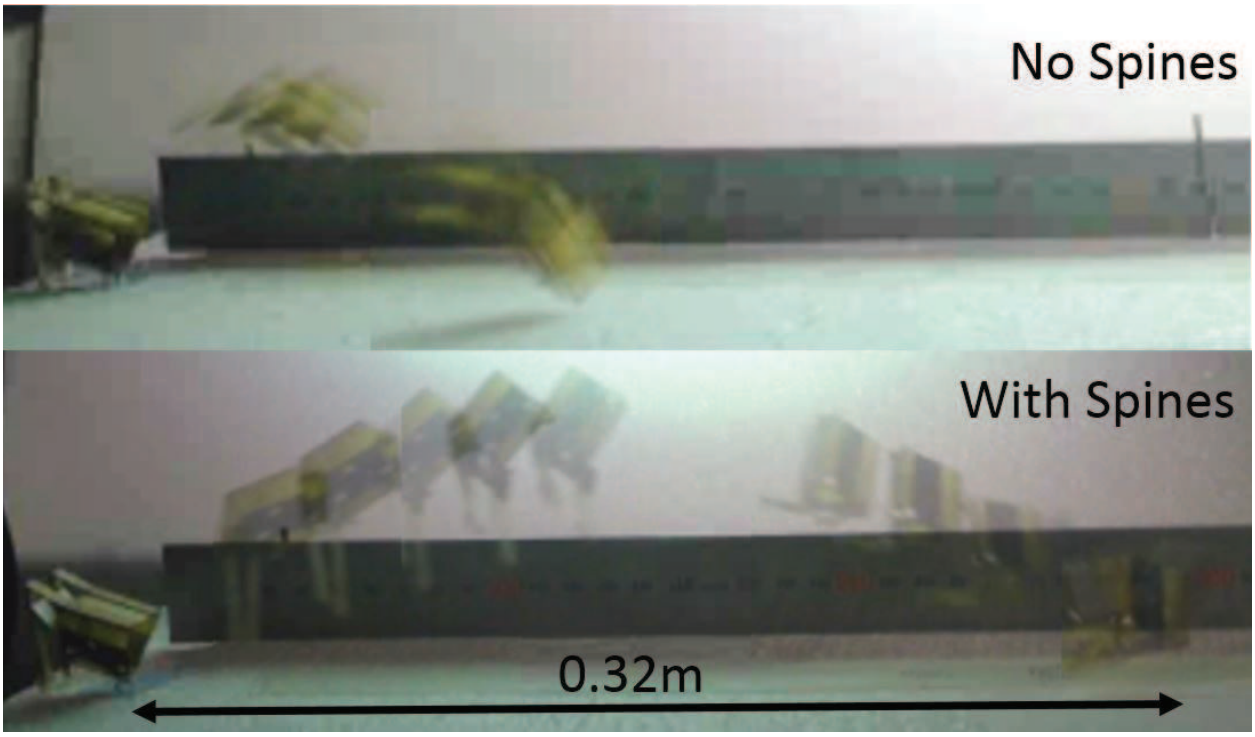


Figure 4.4: Sequential pictures of the robot jumping on Styrofoam where the top is without spines and the bottom is with spines.

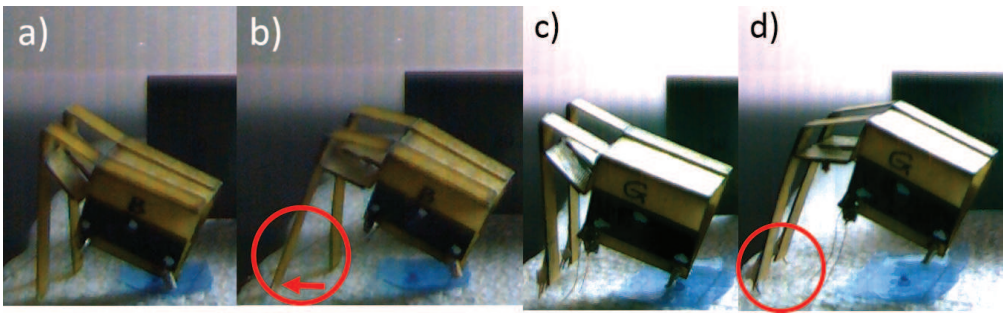


Figure 4.5: The robot without spines (a&b) and with spines (c&d) jumping on Styrofoam where a&c is immediately before triggering and b&d is immediately after triggering.

the robot closer to the no-slip model (Table 4.1). The rotational velocity also decreased by 58%, making the robot more stable in flight.

Table 4.1: Kinetic Energy of the Robot (mJ) at Takeoff

| Surface Type | No Spines or Attachment Pad | Spines | Spines and Attachment Pad |
|---|---|---|---|
| Styrofoam | 3.6±1.1 | 6.0±0.5 | 7.1±0.6 |
| Sandpaper | 6.4±0.2 | 5.8±0.2 | 8.0±0.2 |
| Teflon | 0±0 | 0±0 | 7.8±0.3 |
| No-slip Model | N/A | 6.6 | 7.9 |

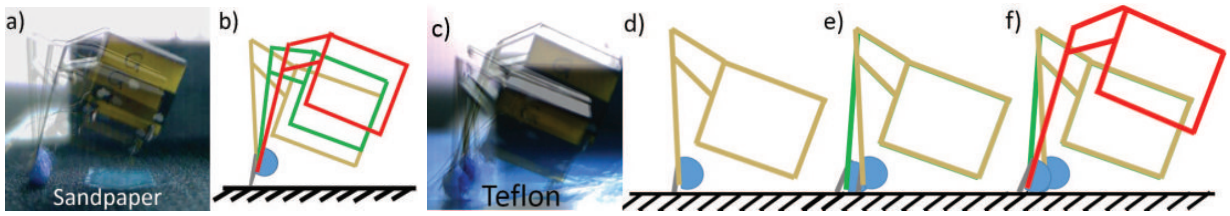


Figure 4.6: Launch kinematics of robot with spine and attachment pad jumping on sandpaper (Left) and Teflon (Right). a,c) Overlaid frames of the video at different times. b,d-f) Outline of the robot, spine, and attachment pad at different frames. Brown is the first frame, green is the second, and red is immediately before takeoff.

## Jumping of the Robot with Spines and Attachment Pad

To evaluate the attachment pad's utility, tests were conducted using the robot with spines and an attachment pad on six different surfaces: Teflon, Styrofoam, and four different grit sizes of sandpaper (2000, 400, 220, and 60). It should be noted that the particles on the sandpaper are larger as the grit size gets smaller. From the high speed video, I found spines are effective on rough surfaces, such as sandpaper of grit sizes 60, 220, and 400. The spines engage the surface at the initiation of jump and do not slip (Fig. 4.6 a-b). However for smooth surfaces (such as Sandpaper 2000, Styrofoam, and Teflon) the spines slip far enough to allow the attachment pad to engage the surface. This is seen more clearly in Fig.4.6 c-f, where the leg slips from d to e.

The kinetic energy on Sandpaper 60cw is the highest at 8.0mJ, which is close to the model (7.9mJ) and an increase from the control case (6.4mJ) (Table 4.1). The kinetic energy on Teflon is the next highest at 7.8mJ, a large increase from 0mJ. The kinetic energy on Styrofoam increased from the control case (3.6mJ) and the robot with just spines (6.0mJ) to 7.1mJ.

To analyze the reaction forces of the modified robot, the robot jumped three times each on sandpaper, Styrofoam and Teflon attached to a force sensor (Fig.4.7). In all trials the horizontal force was larger than the vertical force, similar to forces from the model in Fig.4.2. The largest vertical forces were on Styrofoam while the lowest horizontal forces were on

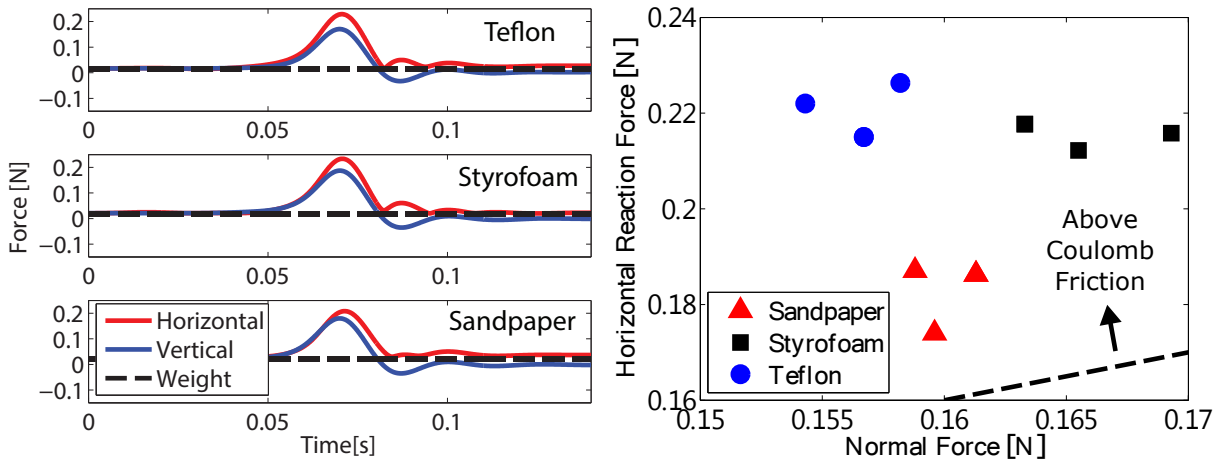


Figure 4.7: (Left) Reaction forces obtained from the force sensor for a robot jumping on Teflon, Styrofoam and sandpaper. (Right) Plot of peak vertical reaction forces with respect to horizontal reaction forces for all trials.

sandpaper.

## 4.4 Conclusions

The bio-inspired spines and attachment pads evaluated in this chapter changed the performance of the robot depending on the surface. On Styrofoam, the spines increased kinetic energy by 65%, which is closer to the no-slip model (6.6mJ). However the spines did not alter the robot's performance on sandpaper significantly, or Teflon where the robot with or without spines could not jump at all. The attachment pad was added to allow the robot to jump on Teflon and the kinetic energy increased from 0 to 7.8mJ. The robot also utilized the attachment pad on smooth surfaces such as Styrofoam and sandpaper 2000Cw, while continuing to use the spines on surfaces with larger asperities. The addition of the attachment pad also increased the kinetic energy of the robot on Styrofoam and sandpaper from the case with just spines. Therefore we have shown that the foot type significantly affects jumping performance, and can be tuned for surface characteristics. By utilizing foot characteristics such as spines and attachment pads, we can have passive systems to increase the performance of robots such as those used for search and rescue.

# Chapter 5

# Self-Engaging Spined Gripper for Steep Jumps

## 5.1 Introduction

Due to high impact forces and low duty cycles, monopedal jumping robots are particularly susceptible to failure from a slipping foot. Spines provide a solution to reduce slip, but there has been little research on how to effectively engage them into a surface with a dynamic jumping robot. Previous robots utilizing spines operate in different regimes of surface approach speed and cycle time (Fig. 1.3 in Ch.1). For a penetrable substrate, spines must be directed into the surface at suitable holding angles, then extracted before the foot leaves the ground. This is the first spined gripper kinematically coupled to engage and disengage on a jumping robot. This gripper design adds adhesion and traction capabilities for Salto, a small robot capable of repeated, high-powered jumps [19, 39]. Adhesion is a prerequisite for perching, useful for surveillance and rationing energy. Higher traction enables the robot to jump at both steep and shallow angles without encountering an irrecoverable slip, allowing navigation over tall obstacles as well as under low overhangs.

## 5.2 Gripper Design

Designing a self-engaging gripper mechanism involved (A) kinematically coordinating leg configuration to gripper engagement, (B) calculating spine mounting, and (C) prototyping, as described in the following.

### Kinematic Coordination

The aim was to design a gripper for Salto that is kinematically constrained to engage when the leg crouches and disengage when the leg extends. In particular, the gripper should move to an engaged configuration as the robot begins to crouch, then to remain engaged

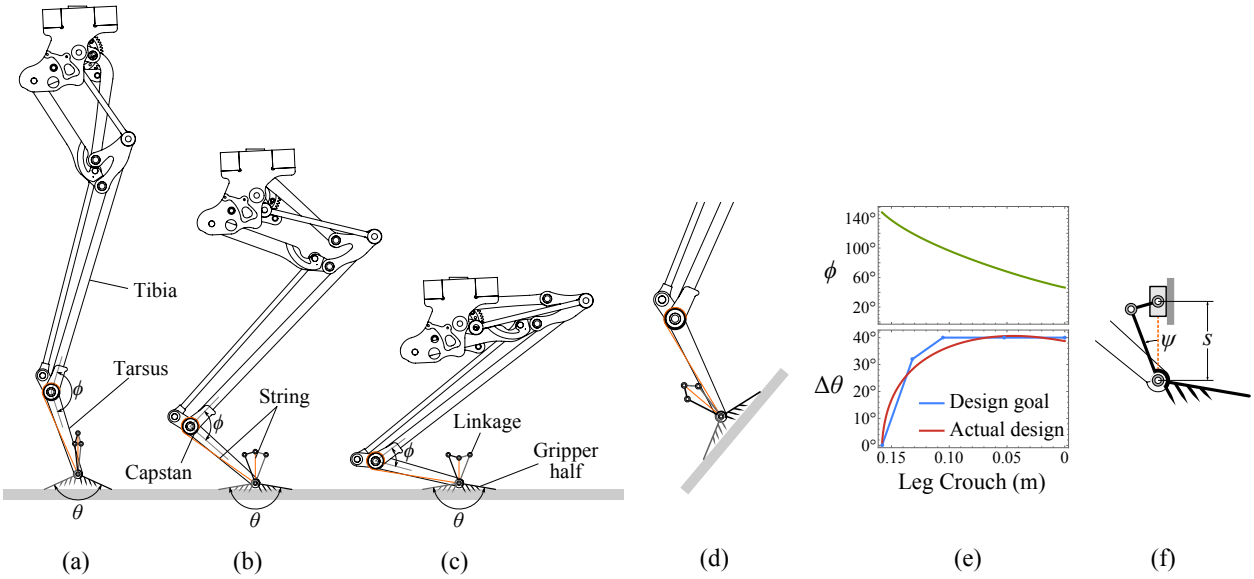


Figure 5.1: Schematic of a Salto leg mechanism modified with a kinematically coordinated gripper. (a) The gripper is disengaged when the leg is extended, (b) then engages and (c) remains engaged for various degrees of crouch. (d) Despite coupling engagement to leg crouch, gripper orientation remains decoupled to be defined by incline angle. (e) The kinematic task involves coordinating the tibia-tarsus angle $\phi$ to a gripper open/close angle $\theta$. (f) This coordination is accomplished by modelling one half of the gripper as a slider-crank function generator.

for all other leg configurations, see Fig. 5.1(a)–(c). Moreover, gripper orientation must be decoupled from engagement motion, allowing the contact angle with a surface to define this additional degree-of-freedom, Fig. 5.1(d). To attain these goals, the relative angle between the tibia and tarsus links, labelled as $\phi$ in Fig. 5.1, is used as a generator of motion at the tarsus. A string that connects to the tibia-tarsus joint routes to the topmost pin of the linkage where it acts as a linear actuator, pulling the top pin toward the central pin and opening two gripper halves. The opening action engages spines into the surface. As the leg uncrouches this process is reversed; the string relaxes and a rubber band pulls the gripper halves together, disengaging the spines and pushing the top pin away from the central pin.

The linkage and tarsus form a two degree-of-freedom five-bar. The joints connecting each gripper half to the tarsus are made coincident, decoupling gripper orientation from its open/close motion. The remaining design challenge is to choose linkage dimensions such that the open/close motion is coordinated with leg extension. The tibia-tarsus angle $\phi$ is a function of leg extension which is proportional to string travel transmitting linear motion to the top joint of the linkage. Angle $\phi$ is plotted in Fig. 5.1(e) along with the desired coordination between leg extension and gripper abduction angle $\Delta\theta$. To achieve this coordination, one half of the linkage may be considered as a slider-crank function generator, Fig. 5.1(f),

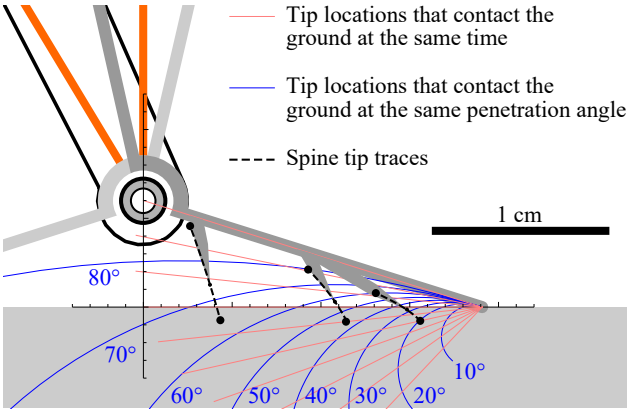


Figure 5.2: Analyzing the space of elliptic traces from [31] discovers a family of constant contact angle arcs from which we choose spine tip locations and angle spines accordingly.

coordinating input string travel $s$ to an output angle $\psi$ that measures the orientation of a gripper half. Following the procedure of [38], we designed the link proportions shown in Fig. 5.1(f) that produce the desired dwell function with $\Delta\theta$ shown in Fig. 5.1(e).

## Directed Spine Velocities

Strategies for engaging spines include catching asperities [1], pinching material [37], and penetrating the substrate [41]. As our focus is the latter, we require that the opening motion of the gripper results in spines piercing the substrate. To accomplish this, spines were mounted onto the gripper so that they point along their velocity vectors at the moment of entering the substrate. The model for spine tip mounting was made by Mark Plecnik and can be found in the proceedings of IEEE International Conference on Robotics and Automation 2018 [31]. A diversity of penetration angles were selected in order to engage a variety of substrates. Those angles, depicted in Fig. 5.2, are 74.0°, 57.4°, and 32.7°.

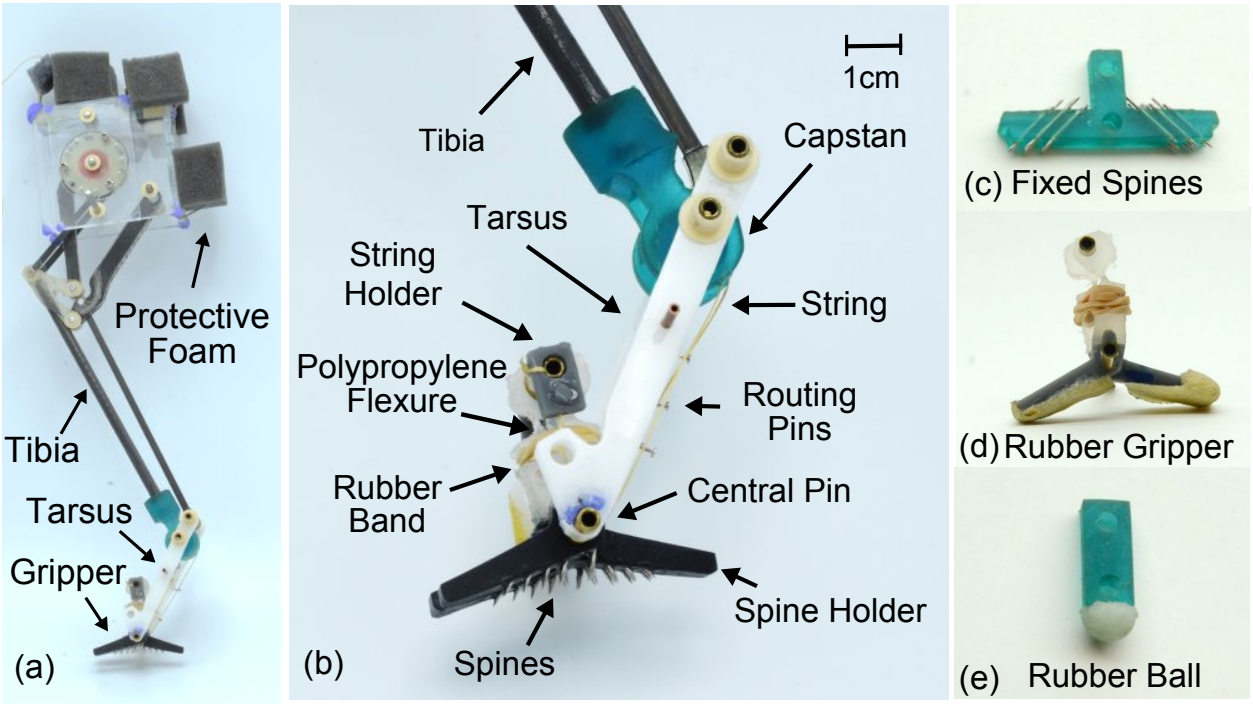


Figure 5.3: (a) Salto Body with gripper attachment. (b) Gripper with spines attached to the robot. (c) End effector with spines held fixed at 43° from horizontal. (d) Gripper with rubber attached to the bottom instead of spines. (e) 3D printed end effector with a rubber hemisphere attached (referred to as a *rubber ball*).

## Manufacturing

The gripper is made up of three subsystems: the capstan, the string subsystem, and the linkage. The capstan is 3D printed and attached to the base of the tibia (Fig. 5.3(b)). The string subsystem consists of the pins, string tightener, and an aramid fiber string. There are two large pins: the central pin located at the bottom of the tarsus that the linkage is free to rotate around, and the topmost pin of the linkage that gets pulled toward the central pin when the linkage is actuated. Smaller routing pins are inserted into the tarsus to guide the string from the capstan to the central pin. Routing pins ensure the string does not interfere with the swing motion of the linkage through the tarsus and direct string tension so as to return the linkage to a centered orientation when it is not in ground contact. The string originates from the capstan and terminates into string holders that sit on either side of the topmost pin. These string holders have a cylinder that the end of the string twists around, thereby removing any slack in the string.

There are three separate linkage halves for force balancing. The top of a linkage half consists of a milled out polypropylene piece with a hole to connect to the topmost pin and a flexure that acts as a joint. The polypropylene also acts as a return spring by pushing the

top pin away from the central pin until a rubber band takes over. The polypropylene is glued to a 3D printed piece with holes to direct the exact angle of the spines. To control the length of the spines during assembly, a 3D printed fixture was used to accurately position spine tips to certain heights. After sliding the spines through their mounting holes and positioning them with the fixture, they are glued in place.

A first spined gripper was constructed with spines angled according to the model in Fig. 5.2, where there is a combination of steep spines for penetrating a surface [41] and shallow spines to engage along the surface for traction [1]. A second spined gripper specializes in adhesion forces and has steeper and longer spines for better penetration. Several other foot designs were constructed to serve as controls that were tested against (Fig. 5.3(c)-(e)), including an end effector with fixed spines, a gripper covered in rubber, and an end effector with a rubber hemisphere at the end (referred to as a *rubber ball*).

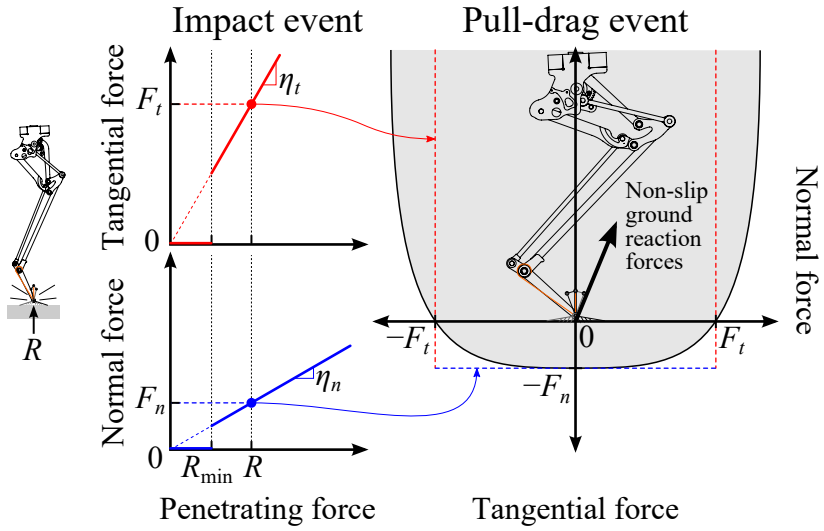


Figure 5.4: At the time of impact, spines penetrate into a substrate, affording a space of non-slip ground reaction forces during a pull-drag event in the future. The coefficients of engagement, $\eta_t$ and $\eta_n$, model maximal non-slip tangential $F_t$ and adhesive $F_n$ forces as proportional to the previously occurring impact $R$. This model is only valid if a threshold penetrating force $R_{\min}$ is surpassed.

## 5.3 Coefficient of Engagement

An obvious candidate for measuring ground contact engagement is the coefficient of friction. However, this quantity does not describe the adhesive loads which are readily apparent of penetrated spines. Furthermore, the ground reaction force for this gripper has a history dependent aspect to it: a spine embedded at the time of an impact defines the range of ground reaction forces possible during a normal of tangential loading event in the future, see Fig. 5.4. Therefore, in order to characterize the performance of a penetrating gripper, I propose the *coefficient of engagement* ($\eta_n$ and $\eta_t$), defined by the ratio of a maximal statically generated normal load $F_n$ or tangential load $F_t$ to the impact force $R$ which enabled that load in the first place. Furthermore, we require $R$ to be greater than the minimum impact $R_{\min}$ required for penetration.

Unlike friction, our definition relaxes the requirement for a normal force to be present in order to measure a tangential force. Instead, tangential and normal reaction forces are proportional to a previous impact force, allowing tangential loading in the absence of normal force or adhesion in the absence of a tangential load. The assumption of proportionality is based off previous work by [41], as well as handbook guidelines on fastener extraction [4]. In the case that impact and tangential loading do proceed simultaneously, then coefficient of engagement in the tangential direction degenerates into coefficient of friction. This is the case with dynamic loading events such as the stance phase in between jumps.

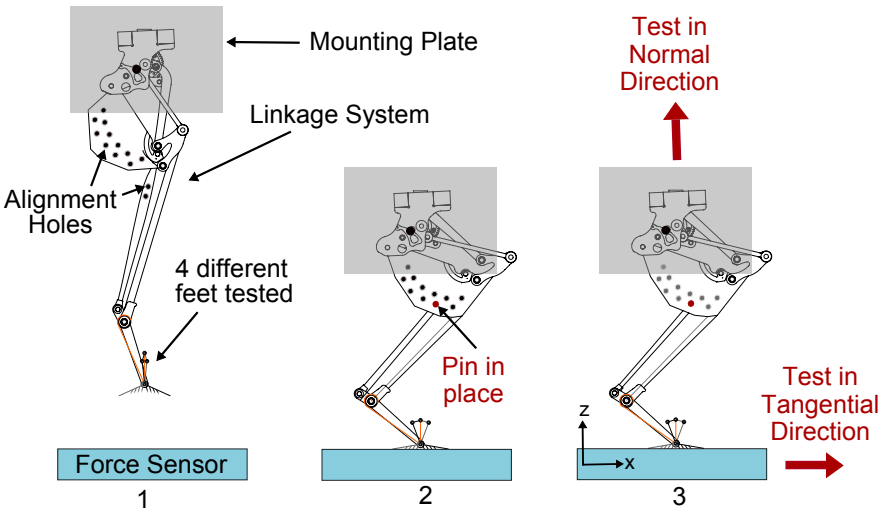


Figure 5.5: Static testing procedure to find CoE. 1) The leg is lowered onto the force sensor. 2) The leg is lowered to a certain amount of crouch and pinned in place. 3) The leg is slowly pulled in the normal or tangential direction.

## 5.4 Static Engagement

### Methods

To experimentally determine the coefficient of engagement (CoE) for the gripper mechanism, the gripper was attached to a Salto leg made out of delrin. It should be noted that for all our CoE tests the first spined gripper was used, which has a larger range of spine angles. The leg contains alignment holes in two links so that when the links pass in front of each other, the leg could be constrained with a pin (Fig. 5.5). The holes were positioned to test the CoE's for different stages of crouch. This leg was attached to a platform that could be controlled in the vertical ($z$) direction and utilized spring loaded linear bearings for force control in the vertical and horizontal ($x$) directions. Sample material was attached to the force sensor (ATI Mini45) which was bolted onto a platform that could be controlled in the $x$-$y$ plane. The test procedure is shown in Fig. 5.5 where the leg is lowered onto a force sensor, pinned in a certain crouched position, and pulled in the tangential or normal direction to the surface.

The spined gripper was tested against the fixed spines, a gripper covered in rubber, and a rubber ball, all tested at different stages of crouch (Fig.5.3c-e). The different materials used were cork, rigid open-celled foam, acrylic, and sandpaper to get a variety of surfaces that vary on the scales of amount of asperities and penetrable versus impenetrable. Each test that varied on end effector type, crouch amount, and surface material was repeated three times. An example set of force sensor data for a CoE test in tangential loading and adhesion can be seen in Fig. 5.6. CoE was calculated by taking the maximum force needed to disengage the end effector from the surface divided by the penetration force needed when first engaging the end effector to the surface.

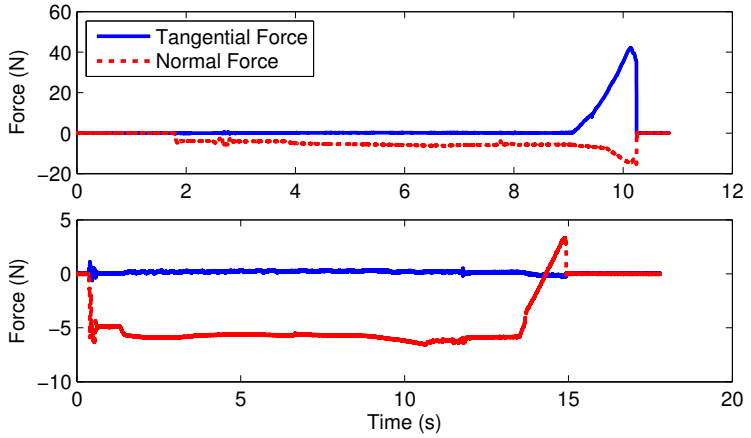


Figure 5.6: Force sensor data from the static test in the tangential (top) and normal (bottom) directions. Both tests were conducted on cork at 70% crouched.

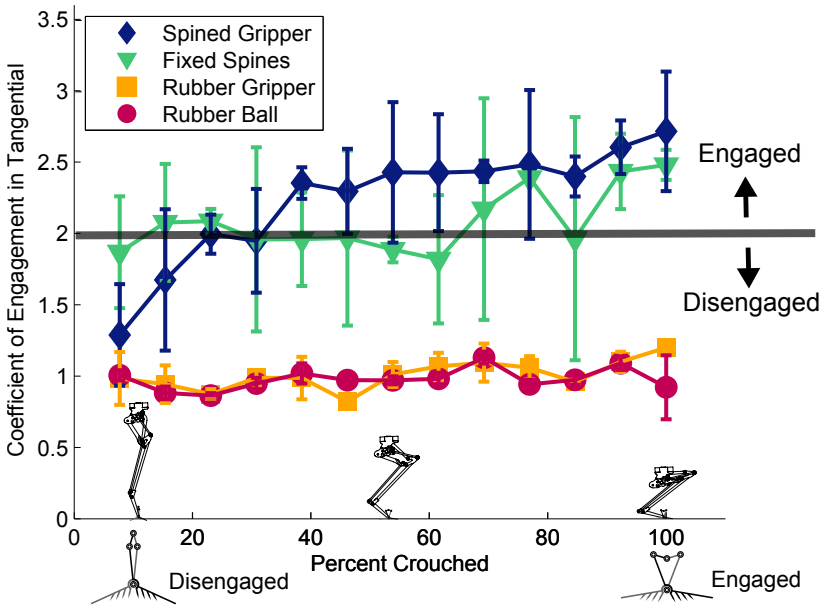


Figure 5.7: Coefficient of engagements taken from static testing on cork. CoE is plotted versus how crouched the leg is, where to the left it is fully extended and to the right it is fully crouched. The gripper diagram on the bottom left illustrates how the gripper is disengaged when the leg is uncrouched, and the spines aren't able to penetrate the surface. But on the right the gripper is engaged and the spines dig into the surface. The engaged/disengaged line highlights how the spined gripper is disengaged from the surface and has a low CoE up until it is over 30% crouched.

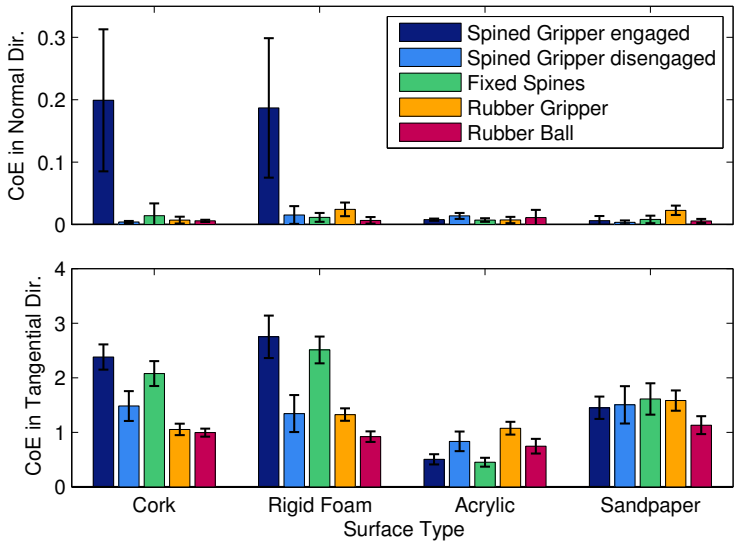


Figure 5.8: Static testing for CoE in normal and tangential loading for all end effectors and surfaces after being statically engaged.

## Results

An example set of data on cork can be seen in Fig. 5.7 where there were high CoE's for the spined gripper and fixed spines, but low values for the gripper with rubber and the rubber ball. Although both spined gripper and fixed spines have high values, the gripper has a method of disengaging from a material by simply uncrouching, as shown by the values when the gripper is less than 30% crouched. Since the other end effectors showed similar performance no matter the amount crouched, we were able to average the CoE values for fixed spines, the rubber gripper, and the rubber ball respectively into Fig. 5.8. For the spined gripper we averaged the CoE depending on whether it was below 30% crouched (disengaged) or over 30% (engaged). In the normal direction (Fig. 5.8), only the engaged spined gripper exhibited a substantial coefficient of engagement on cork and rigid foam. This indicates that while the leg is crouched, the gripper provides the robot with adhesion. Performance on impenetrable surfaces (acrylic and sandpaper) was similar for all end effectors, but in the tangential direction the rubber gripper engages the most on acrylic because it has a high amount of rubber contacting the surface. In the tangential direction, the engaged spined gripper and the fixed spines have high CoE's on the penetrable surfaces (cork and rigid foam), but when the gripper is uncrouched it can function more like a rubber ball and can disengage from a surface. The spined gripper while crouched showed a 1.4 times improvement over a simple rubber ball on cork and a 2 times improvement on rigid foam.

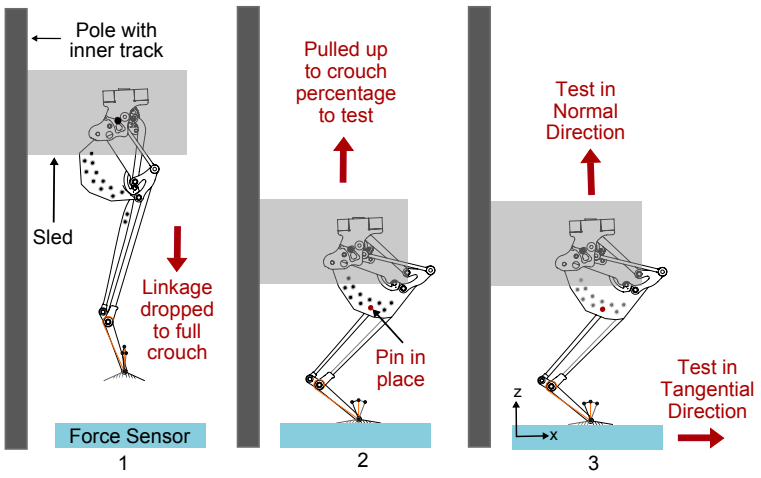


Figure 5.9: Drop testing procedure for CoE. 1) Leg system is dropped from 34cm to the force sensor into a fully crouched position. 2) The sled is raised, allowing the leg to extend to the specific percentage of crouch that is being tested. Then the leg is pinned in place. 3) The leg is pulled in either the normal or tangential direction.

## 5.5 Dynamic Engagement

To verify that the gripper performs in a dynamic application, I first tested its ability to dynamically engage with a surface. The leg used in the static tests was attached to a sled connected to a linear bearing in a tall pole with an inner track. The test procedure can be seen in Fig. 5.9. In order to make sure the leg did not bounce back up, the leg acted as an overdamped system by adding a rubber band to bias it toward being extended and increased its body mass with the sled. An example data set for the drop test in tangential and normal directions is shown in Fig. 5.10.

The CoE was lower for these dynamic tests due to additional oscillations during spine engagement. The crouched spined gripper increased the CoE in the tangential direction by 3 times on cork and 1.5 times on rigid foam compared to the rubber ball. Again, the CoE in the normal direction was substantial for the spined gripper on cork and rigid foam during dynamic engagement tests (Fig. 5.11). The fixed spines and rubber gripper were also able to develop some adhesive forces on foam. The uncrouched spined gripper was able to disengage material during dynamic engagement tests. These CoE values are used in the dynamic model in Section 5.6 to predict how different feet should perform on a dynamic, jumping robot.

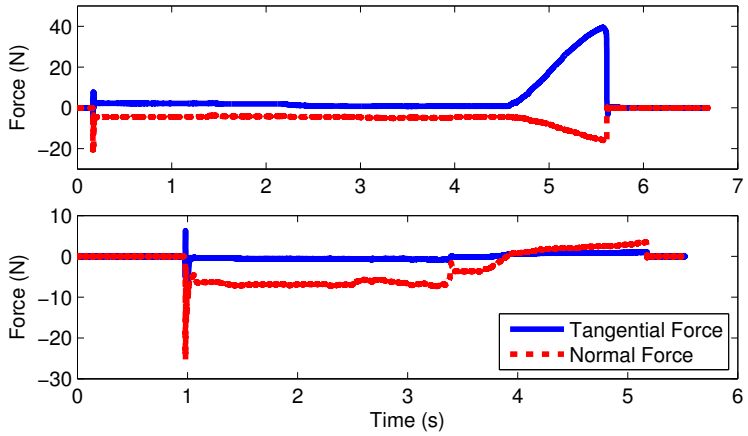


Figure 5.10: Force sensor data from the dynamic engagement test in the tangential (top) and normal (bottom) directions. Both tests were conducted on cork at 70% crouched.

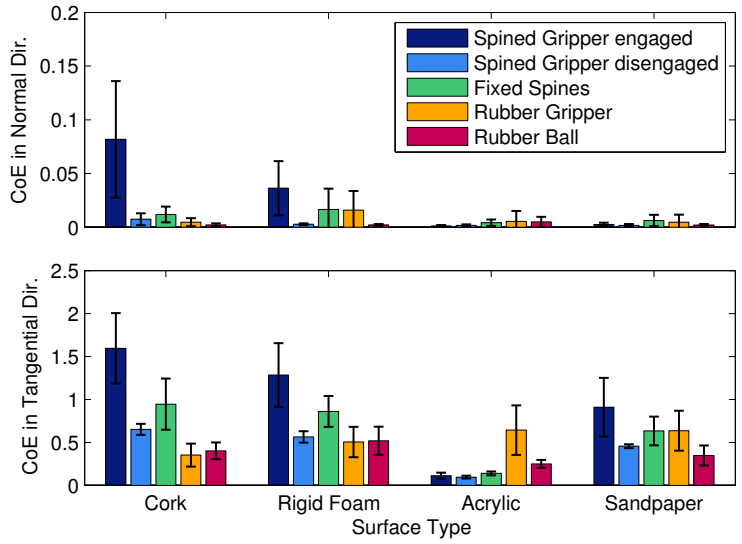


Figure 5.11: Dynamic engagement testing for CoE in normal and tangential loading for all end effectors and surfaces after being dynamically engaged.

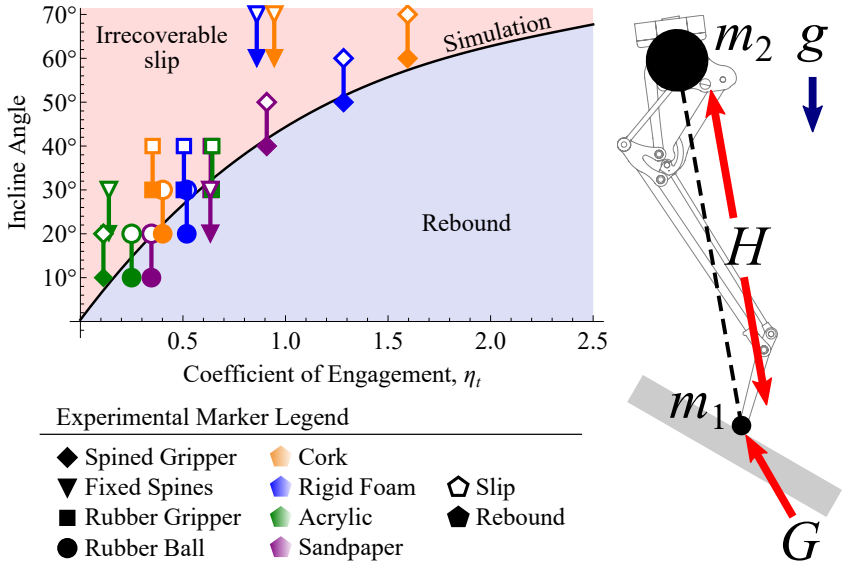


Figure 5.12: (Left) A comparison of the simulation and experimental results displaying the maximum incline angle on which a gripper with a certain dynamic tangential coefficient of engagement may successfully execute a rebound jump. The area under the curve represents the space of successful rebounds indicated by simulation. Plot markers indicate experimental results. Successful rebounds occurred at filled markers and irrecoverable slips occurred at open markers. (Right) Free-body diagram used for dynamic simulation. Force $H$ follows Salto's variable mechanical advantage curve presented in [39].

## 5.6 Simulation of Dynamics

In order to understand CoE from a task level, we simulated rebounds onto inclined planes to find the relationship between coefficient of engagement $\eta_t$ and maximum incline angle, see Fig. 5.12. A gripper with $\eta_t = 1.0$ falling 0.5 m may at best rebound off a 44° angle, whereas $\eta_t = 2.0$ yields a 63° angle.

This result was computed from the two mass model shown in Fig. 5.12, where $m_1$ represents the robot's foot and $m_2$ represents the body. The normal component of contact dependent force $G$ includes a stiffness of $10^4$ N/m and damping coefficient of 20 Ns/m. The tangential component models $\eta_t$ as Coulombic friction. $H$ is modelled from the force profile and variable mechanical advantage of Salto's leg, printed in Fig. 10 of [39], and additionally includes internal friction and damping multiplied by configuration-dependent mechanical advantage. For more details refer to Mark Plecnik's work in [31].

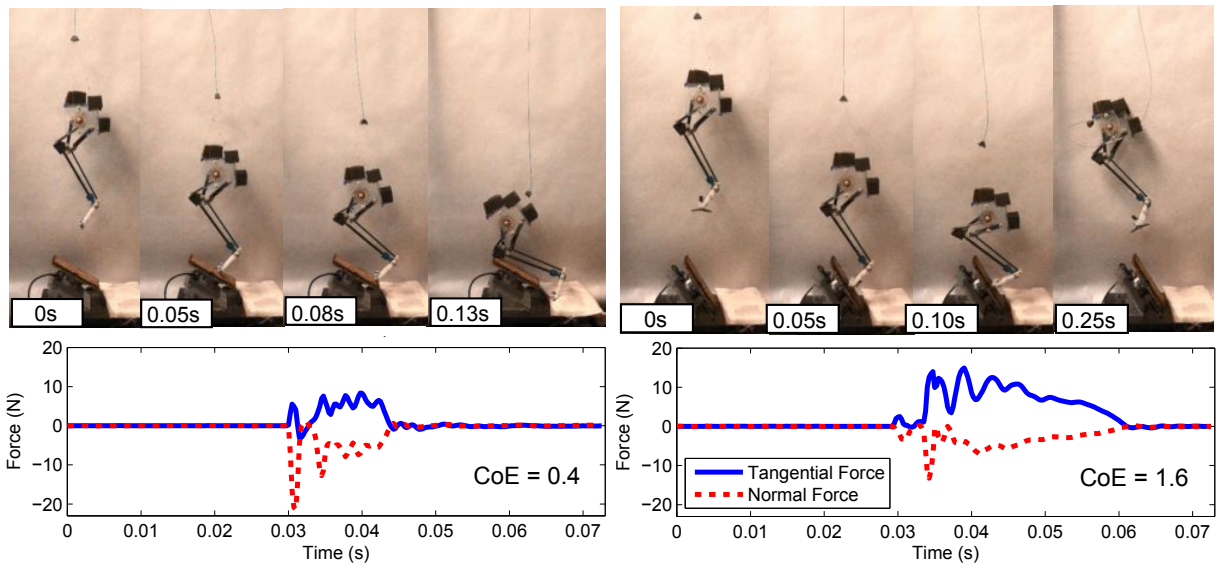


Figure 5.13: (Left) Video stills of the robot with a rubber ball slipping off cork at 30° with the force sensor data underneath. (Right) Video stills of the robot with the spiny gripper jumping off cork at 60° with the force sensor data underneath.

## 5.7 Jumping Experiments

After verifying the gripper's ability to dynamically engage, the gripper ability to dynamically release from the surface was tested. To test its ability to disengage, a free drop test was constructed where the body was hanging by a releasable string, dropping the robot by 50cm. The body nested into a fixture at the start to guarantee the same orientation every drop. The robot body was constructed with actual Salto body parts including the latex spring, so when the robot dropped it would crouch, wind the spring and jump back up (Fig. 5.3a). This Salto skeleton weighed 80g, and an additional 57.7g was placed on the body to better mimic the loading of a full Salto assembly and balance out the added gripper weight to minimize angular momentum during jump. To quantify each end effector's performance on cork, rigid foam, acrylic and sandpaper, the Salto skeleton was dropped onto fixed inclined surfaces. Video stills from two example jumps can be seen where the rubber ball slips on 30° and the spiny gripper jumps on 60° (Fig. 5.13). A close up view of the gripper engaging the surface in another trial can be seen in Fig. 5.14.

Experimental results are plotted alongside free drop simulation results in Fig. 5.12. Data points mark measured dynamic CoE values versus the maximum experimental rebound angle for 16 different gripper/substrate combinations. Each maximum rebound angle is presented within a range between a lower bound (filled marker) and upper bound (open marker). Lower bounds were established by completing 3 out of 5 successful rebounds, and upper bounds

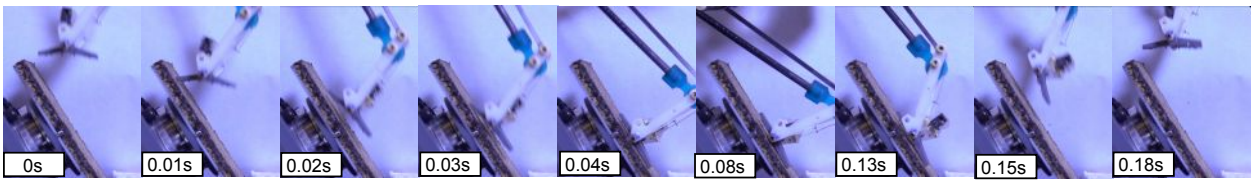


Figure 5.14: Video stills of the spined gripper jumping off cork at 60°. At 0.01s the gripper hits the cork and starts rotating towards the surface. At 0.04s it engages the surface and starts to crouch. By 0.13s the robot has crouched down, un-crouched, and is just about to jump off the surface. At 0.18s the gripper has successfully rotated itself back to its neutral position.

were established when this did not happen. Incline angles were tested in 10° increments. Simulation details were described in Section 5.6.

Here fixed spines seemed to outperform the spined gripper and the dynamic simulation. Although fixed spines yielded a lower CoE than the spined gripper during the dynamic engagement tests, they were able to jump at higher inclines than expected. This is partially explained by their freely rotating end effector. This end effector was able to rotate onto steep surfaces faster than the spined gripper halves, which were slowed by string tension from the capstan mechanism. Also, steeper test angles increased the tangential component of the insertion force to nicely match the angle of the fixed spines.

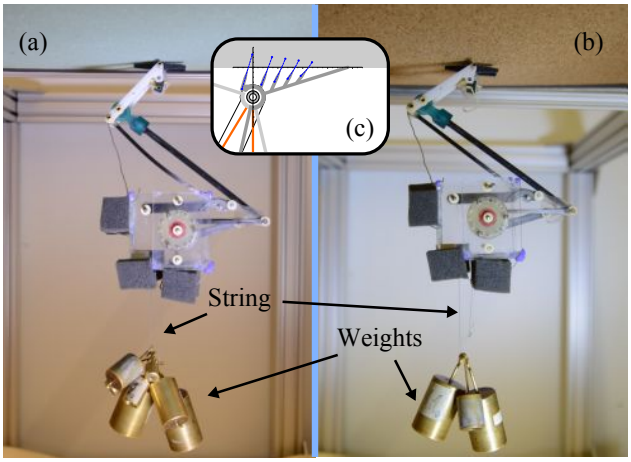


Figure 5.15: Salto skeleton with spiny gripper design adhered to (a) rigid foam and (b) cork with additional weight hanging from its body.

## 5.8 Adhesion Experiments

Although the static tests with the current spined gripper demonstrated the capability to perch onto penetrable substrates, preliminary experiments were conducted to test the spined gripper's ability to adhere to a ceiling. Using the design principles from Section 5.2 and knowledge obtained from our experiments, a second spined gripper was constructed that had steeper angles and longer spines to better penetrate surfaces (Fig. 5.15c). The gripper was attached to the Salto skeleton and crouched onto a ceiling of either rigid foam or cork. The leg was latched in place to keep the robot crouched. Then weights were added until either Salto fell or we reached the weight limit that puts Salto's body near breaking stress. There were eight trials performed for cork and five for rigid foam. The robot was able to carry $433 \pm 35g$ additional weight on cork and $514 \pm 79g$ on rigid foam (Fig. 5.15). Rigid foam reached the weight limit of $600g$ twice. The variation in weight supported was caused by surface variation and the sway of hanging weights, allowing the spines to slip out.

## 5.9 Discussion and Conclusion

In this chapter a gripper mechanism with spines was presented to be used on Salto, a highly dynamic robot. This is the first work to demonstrate spines on a jumping robot that can dynamically penetrate and release from a surface. The gripper's function is dependent on its kinematic design. Energy from landing impacts is transformed through the robot's crouching motion to direct spines into penetrable surfaces at angles that match their velocity vectors. Release from a surface is allowed by coupling spine disengagement to the uncrouching motion of Salto. To measure surface engagement, the coefficient of engagement was introduced, which describes the range of possible ground reaction forces enabled by a previously occurring impact event. The spined gripper increased the tangential CoE by 1.4 times on cork and 2 times on rigid foam compared to the control case of a rubber ball. The additional traction enabled by this improvement allowed the robot to jump off 60° inclines on cork and rigid foam, as opposed to just 20° with a rubber ball, matching our dynamic model. The gripper design also enables adhesive loads, allowing the robot to hold 6.3 times its body weight on cork and 7.5 times on rigid foam. This work details a new strategy for managing the ground reaction force of jumping robots, with a particularly focus on mitigating slip scenarios on penetrable surfaces.

# Chapter 6

# Conclusion and Future Work

## 6.1 Conclusion

In this work I present a passive mechanical design strategy that improves the performance of running and jumping robots without adding additional control or actuators. The basis of this strategy was to use leg spines that can catch the asperities or penetrate a surface. Spines are one of the interlocking methods from biology that can work in unclean environments, support many different body sizes, and can last many cycles. Spines have been used in climbing and perching robots before, however I wanted to use spines to operate on stance timescales shorter than perching robots and dynamically approach surfaces unlike climbing robots.

Spines in this work improve the performance of both running and jumping in robots and biology. Anisotropic and collapsible leg spines improved the foot friction in a palm sized running robot, increasing the speed, maximum incline it could traverse, the amount it could pull, and the robot's energy efficiency. Cricket tibia spines were tested and found to be useful on penetrable substrate. This led to the first spines placed on a jumping robot, which increased its kinetic energy and doubled the distance it could jump. Next I tested spines in a gripper mechanism for a monopedal robot capable of dynamic, high-powered, repeated jumps. This gripper was kinematically coupled to engage/disengage as the leg crouched/uncrouched and took advantage of the high impact speeds to penetrate the substrate. This added traction allowed the robot to jump off higher inclines than a rubber ball foot, 60° as opposed to just 20°. The spined gripper also gave the robot adhesive capabilities, demonstrating it could adhere to a ceiling of penetrable substrate and support 7.5 times its body weight.

Table 6.1: Estimated maximum acceleration of different end effectors, robots, and surface type

| Robot Platform | Robot Mass | End Effector | Material | Est. Max Accel. ($m/s^2$) |
|---|---|---|---|---|
| VelociRoACH | 30g | Fiberglass Spines | Cork | 7 |
| Flea-inspired | 2g | Fiberglass Spines | Styrofoam | 109 |
| | | | Sandpaper | 94 |
| | | | Teflon | N/A |
| Flea-inspired | 2g | Rubber Pad | Teflon | 113 |
| Salto | 100g | Steel Spined Gripper | Cork | 437 |
| | | | Rigid Foam | 406 |
| | | | Sandpaper | 223 |
| | | | Acrylic | 75 |
| Salto | 100g | Steel Spines | Cork | 224 |
| | | | Rigid Foam | 216 |
| | | | Sandpaper | 222 |
| | | | Acrylic | 38 |
| Salto | 100g | Rubber Ball | Cork | 73 |
| | | | Rigid Foam | 69 |
| | | | Sandpaper | 92 |
| | | | Acrylic | 55 |

To summarize and compare my work on improving millirobot traction, I decided to compare the different end effectors by using Estimated Maximum Acceleration (EMA) which is the highest measured traction force divided by the mass of the robot platform used. The results are shown in Table 6.1 where the VelociRoACH has the lowest measured EMA at $7m/s^2$, but in this application the fiberglass leg spines were only used for horizontal traction. The flea inspired robot had a higher EMA and used the fiberglass leg spines in a jumping application, however it could not jump on Teflon. These fiberglass leg spines improved the robots' performance on cork and styrofoam compared to the robot without leg spines. Adding rubber foot pads allowed it to jump on teflon, giving it a high EMA of $113m/s^2$. Steel was used instead of fiberglass in my PhD work to support more dynamic thrust forces and impact forces of around $60N$. The steel spines and steel spined gripper for the Salto robot had similar EMA's for sandpaper at $222m/s^2$ and $223m/s^2$. However because the steel spined gripper was able to engage and grip the surface, it had a higher EMA of $437m/s^2$ and $406m/s^2$ on cork and rigid foam compared to the steel spines. On all surfaces the steel spined gripper performed better than the rubber ball on Salto.

This work demonstrates the performance of two different types of spines on different ends of the spectrum, compliant spines for asperity catching and hard spines for surface penetration. For a lightweight, smaller robot, using compliant leg spines improved performance

as the compliance allows the spine to travel along the surface until it catches an asperity. Catching the asperity is all that is needed because the asperity can support the force that the small robot uses to propel itself forward. However, heavier robots or robots that have large impact forces would need hard spines. This way the spine won't break and would be able to support the weight. It is also beneficial for the spine to be able to penetrate the surface because that creates its own hold to support larger contact forces and the spine won't bounce off the surface in dynamic applications. Being embedded in the surface would also better support the moments caused by a larger robot's center of mass farther from the surface.

## 6.2 Future Work

Future work will involve integration of the spined gripper with a motorized Salto robot. With a spined gripper the robot will be able to jump off steep inclines and jump forward using shallow angles. This allows the robot to navigate over tall obstacles as well as under low overhangs, making this a very capable robot that can tackle all sorts of non-ideal environments. Eventually we hope to use the spined gripper for perching and rapid engagement and disengagement for steep surfaces that don't contain footholds, enabling wall jumps to progress up a shaft or using the walls to jump down a hallway to avoid rubble on the ground. Perfecting the perching method would also allow Salto to do surveillance or save energy by hanging off a ceiling or vertical surface. Another application of spines is a solution for passive turning in terrestrial robots, since this work demonstrated that spines allow robots to resist torque disturbances. Spines can also be used to control take off angle in jumping. Although spines in this work demonstrated to improve performance on dynamic palm sized robots, spines could be applied to larger robots.

Soft robots could also find spines useful in locomotion and gripping. Classic soft robots that are made up of Soft Pneumatic Actuators (SPAs) that have a skin with a rubbery texture, which they have to fight against to move forward. Spines would give them some anisotropy to allow them to move only in one direction at the time. This could also work in nano-scale robots so that if they were to vibrate, it could move them in one direction, but move them in the opposite direction when vibrated at a different frequency. A soft robot using SPAs could also use use spines for gripping. This could be used as an end effector, so it could surround an object and inflate to engage the spines, or it could cover its body in spines and inflate to activate the spines and stabilize itself. For example, if it was navigating a nook formed by rubble, and an earthquake hit, the robot could inflate completely to engage the spines and wedge itself in place.

Another application for spines are other gripping end effectors. Because spines are anisotropic they can grip and un-grip objects in interesting ways. They could be used for one way sliding transports. There could be an application where it can grab an object and spines hold it in place, or a gripper could hold objects and spines to allow them to slip out when a certain condition is met. This would also be useful in space applications because without gravity, it is useful to have some sort of directional constraint. To hold things in

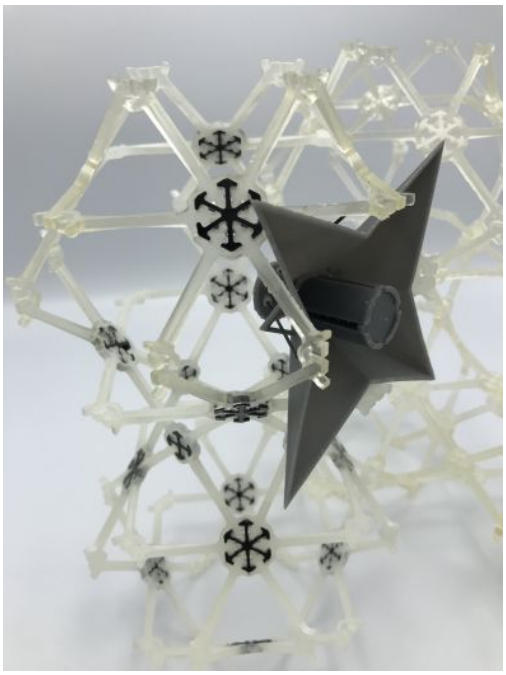

Figure 6.1: End effector with spines for robots to traverse a modular 3D lattice design.

space, more than one boundary object is needed. For example, on earth, a box can be held with just a table because gravity will keep it constrained. However, in space, one would need a table, and a clamp to hold the object on the table. By adding spines to grip an object, you simply need to make contact, instead of applying potentially damaging, crushing hold forces. Spines would make it easy to extract and slip out in one direction, or the spines could oppose movement and hold an object no matter the accelerations applied.

Spines could also be used in other space applications because in minimal gravity there needs to be a strategy to maintain ground contact for locomotion. Simple passive spines on end effectors could be helpful when traversing a surface with plenty of asperities, such as an asteroid. Another way to use spines would be to put them on the feet of a walking robot and use them to engage and traverse the surface of a structure built from truss systems (see Fig 6.1). Preliminary work has been done in collaboration with the Coded Structures Lab at NASA Ames Research Center. Modular structures built from lattice building blocks have high stiffness to weight ratios, which make them desirable for space applications. These building blocks can be assembled and disassembled to be reconfigured into any structure needed. This surface has sparse contact surface area, but the spines can easily engage and support the forces made from the robot walking over the lattice or manipulate lattice building blocks. The spines passively engage the surface which saves energy because there are no actuators used to engage the surface or maintain engagement. These spines for space walking robots also kinematically engage and disengage based on whether the robot is in stride or stance.

# Bibliography


[1] A. T. Asbeck et al. "Scaling Hard Vertical Surfaces with Compliant Microspine Arrays". In: *The International Journal of Robotics Research* 25.12 (2006), pp. 1165–1179. ISSN: 0278-3649. DOI: 10.1177/0278364906072511.

[2] A.T. Asbeck, M.R. Cutkosky, and W.R. Provancher. "SpinybotII: climbing hard walls with compliant microspines". In: *ICRA '05. Proceedings., 12th Int. Conf. Adv. Robot. 2005.* (2005), pp. 601–606. DOI: 10.1109/.2005.1507470.

[3] K. Autumn. "Gecko Adhesion: Structure, Function, and Applications". In: *MRS Bulletin* 32.6 (2007). DOI: 10.1557/mrs2007.80.

[4] E. A. Avallone and T. Baumeister III. *Marks' Standard Handbook for Mechanical Engineers*. Tenth. New York, NY: McGraw Hill, 1996.

[5] M. J. Baum et al. "Anisotropic friction of the ventral scales in the snake lampropeltis getula californiae". In: *Tribology Letters* 54.2 (2014), pp. 139–150. ISSN: 10238883. DOI: 10.1007/s11249-014-0319-y.

[6] P. Birkmeyer, A. Gillies, and R. S. Fearing. "CLASH: Climbing vertical loose cloth". In: *2011 IEEE/RSJ Int. Conf. Intell. Robot. Syst.* (Sept. 2011). DOI: 10.1109/IROS.2011.6094905.

[7] M. Brunner et al. "The FKIE Robot System for the European Land Robot Trial ". In: *Proceedings of the 5th Int. IARP Workshop on Robotics for Risky Interventions and Environmental, Surveillance-Maintenance* (2011).

[8] K. Carpenter, N. Wiltsie, and A. Parness. "Rotary Microspine Rough Surface Mobility". In: *IEEE/ASME Transactions on Mechatronics* 21.5 (2016), pp. 2378–2390. ISSN: 10834435. DOI: 10.1109/TMECH.2015.2511012.

[9] P. Cheng et al. "Cooperative Towing With Multiple Robots". In: *J. Mech. Robot.* 1.1 (2009), p. 011008. ISSN: 19424302. DOI: 10.1115/1.2960539.

[10] Z. Dai, S. N. Gorb, and U. Schwarz. "Roughness-dependent friction force of the tarsal claw system in the beetle Pachnoda marginata (Coleoptera, Scarabaeidae)." In: *The Journal of Experimental Biology* 205 (2002), pp. 2479–2488. ISSN: 0022-0949.

[11] J. H. Dirks, C. J. Clemente, and W. Federle. "Insect tricks: two-phasic foot pad secretion prevents slipping." In: *Journal of the Royal Society, Interface / the Royal Society* 7.45 (2010), pp. 587–593. ISSN: 1742-5689. DOI: 10.1098/rsif.2009.0308.

[12] R. J. Full, J. A. Assad, and C. F. Herreid II. "Economics of cockroaches exercising with loads". In: *Amer. Zool.* Vol. 24:124A. 1984.

[13] R. J. Full et al. "Quantifying Dynamic Stability and Maneuverability in Legged Locomotion". In: *Integrative and Comparative Biology* 42 (2002), pp. 149–157.

[14] K. C. Galloway et al. "X-RHex : A Highly Mobile Hexapedal Robot for Sensorimotor Tasks". In: *University of Pennsylvania Scholarly Commons* (2010).

[15] A. Gillies and R. Fearing. "Shear Adhesion Strength of Thermoplastic Gecko-Inspired Synthetic Adhesive Exceed Material Limits". In: *Langmuir* 27 (2011), pp. 11278–11281.

[16] S. N. Gorb. "Biological attachment devices: exploring nature's diversity for biomimetics". In: *Philosophical Transactions of the Royal Society A: Mathematical, Physical and Engineering Sciences* 366.1870 (2008), pp. 1557–1574. ISSN: 1364-503X. DOI: 10.1098/rsta.2007.2172.

[17] D. W. Haldane et al. "Animal-inspired design and aerodynamic stabilization of a hexapedal millirobot". In: *2013 IEEE Int. Conf. Robot. Autom.* (May 2013). DOI: 10.1109/ICRA.2013.6631034.

[18] D. W Haldane et al. "Integrated Manufacture of Exoskeleton and Sensing for Folded Millirobots". In: *Journal of Mechanisms and Robotics 2015* (2015).

[19] D. W. Haldane et al. "Robotic vertical jumping agility via series-elastic power modulation". In: *Science Robotics* 1.1 (2016).

[20] A. M. Hoover and R. S. Fearing. "Fast scale prototyping for folded millirobots". In: *2008 IEEE Int. Conf. Robot. Autom.* (2008).

[21] L. L. Howell. *Compliant Mechanisms*. New York, NY, USA: John Wiley and Sons, Inc., 2001.

[22] K. Jayaram and R. J. Full. "Cockroaches traverse crevices, crawl rapidly in confined spaces, and inspire a soft, legged robot". In: *Proceedings of the National Academy of Sciences* 113.8 (2016), E950–E957. ISSN: 0027-8424. DOI: 10.1073/pnas.1514591113.

[23] K. Jayaram, C. Merritt, and R. J. Full. "Robust climbing in cockroaches results from fault tolerant design using leg spines". In: *Society of Integrative and Comparative Biology*. Jan. 2012, p. 79.4.

[24] A. Jusufi et al. "Active tails enhance arboreal acrobatics in geckos". In: *Proceedings of the National Academy of Sciences* 105.11 (2008), pp. 4215–4219. ISSN: 0027-8424. DOI: 10.1073/pnas.0711944105.

[25] S. Kim et al. "Smooth Vertical Surface Climbing With Directional Adhesion". In: *IEEE Transactions on Robotics* 24.1 (Feb. 2008), pp. 65–74. ISSN: 1552-3098. DOI: 10.1109/TRO.2007.909786.

[26] M. Kovač et al. "A perching mechanism for micro aerial vehicles". In: *Journal of Micro-Nano Mechatronics* 5.3 (2009), pp. 77–91. ISSN: 18653928. DOI: 10.1007/s12213-010-0026-1.

[27] H. Lee, N. F. Scherer, and P. B. Messersmith. "Single-molecule mechanics of mussel adhesion". In: *Proceedings of the National Academy of Sciences* 103.35 (2006), pp. 12999–13003. ISSN: 0027-8424. DOI: 10.1073/pnas.0605552103.

[28] J. S. Lee and R. S. Fearing. "Anisotropic collapsible leg spines for increased millirobot traction". In: *2015 IEEE Int. Conf. on Robotics and Automation (ICRA)* (2015), pp. 4547–4553. DOI: 10.1109/ICRA.2015.7139829.

[29] J. S. Lee, R. S. Fearing, and K.-J. Cho. "Compound Foot For Increased Millirobot Jumping Ability". In: *Advances in Cooperative Robotics*. World Scientific, 2016, pp. 71–78. DOI: 10.1142/9789813149137_0012.

[30] J. S. Lee et al. "Crickets Jumping from Diverse Substrates Inspire Leg Design in a Millirobot". In: *Integrative and Comparative Biology*. Vol. 57. 2017, E324.

[31] J. S. Lee et al. "Self-Engaging Spined Gripper with Dynamic Penetration and Release for Steep Jumps". In: *2018 IEEE Int. Conf. on Robotics and Automation (ICRA)* (2018).

[32] C. Y. Lin and H. Y. Chueh. "Design and implementation of a wall-jumping robot with climbing claws". In: *Journal of the Chinese Institute of Engineers* 40.1 (2017), pp. 45–54. ISSN: 21587299. DOI: 10.1080/02533839.2016.1259022.

[33] A. Lussier Desbiens, A. T. Asbeck, and M. R. Cutkosky. "Landing, perching and taking off from vertical surfaces". In: *The Int. Journal of Robotics Research* 30.3 (2011), pp. 355–370. ISSN: 0278-3649.

[34] D. Mellinger, M. Shomin, and V. Kumar. "Control of Quadrotors for Robust Perching and Landing". In: *Int. Powered Lift Conf.* (2010), pp. 119–126.

[35] M. Noh et al. "Flea-inspired catapult mechanism for miniature jumping robots". In: *IEEE Transactions on Robotics* 28.5 (2012), pp. 1007–1018. ISSN: 15523098. DOI: 10.1109/TRO.2012.2198510.

[36] B. N. J. Persson. "Wet adhesion with application to tree frog adhesive toe pads and tires". In: *Journal of Physics: Condensed Matter* 19.37 (2007), p. 376110.

[37] M. Plecnik and R. S. Fearing. "A Study on Finding Finite Roots for Kinematic Synthesis". In: *ASME 2017 IDETC/CIE Conf.* Cleveland, OH, Aug. 2017.

[38] M. Plecnik and J. M. McCarthy. "Five Position Synthesis of a Slider-Crank Function Generator". In: *ASME 2011 IDETC/CIE Conf.* Washington, D.C., Aug. 2011.

[39] M. Plecnik et al. "Design Exploration and Kinematic Tuning of a Power Modulating Jumping Monopod". In: *Journal of Mechanisms and Robotics* 9.1 (2016), p. 011009.

[40] M. T. Pope et al. "A Multimodal Robot for Perching and Climbing on Vertical Outdoor Surfaces". In: *IEEE Transactions on Robotics* 33.1 (2017), pp. 38–48. ISSN: 15523098. DOI: 10.1109/TRO.2016.2623346.

[41] W. R. Provancher et al. "Towards Penetration-based Clawed Climbing". In: *Climbing and Walking Robots* 27.2 (2005), pp. 961–970. ISSN: 0143-991X.

[42] S. Rezazadeh et al. "Spring-mass Walking with ATRIAS in 3D: Robust Gait Control Spanning Zero to 4.3 KPH on a Heavily Underactuated Bipedal Robot". In: *Proceedings of the ASME Dynamic Systems and Control Conference* (2015).

[43] J. C. Spagna et al. "Distributed mechanical feedback in arthropods and robots simplifies control of rapid running on challenging terrain." In: *Bioinspir. Biomim.* 2.1 (Mar. 2007), pp. 9–18. ISSN: 1748-3190. DOI: 10.1088/1748-3182/2/1/002.

[44] M. J. Spenko et al. "Biologically Inspired Climbing with a Hexapedal Robot Biologically Inspired Climbing with a Hexapedal Robot". In: *J. Field Robotics* 25.4 (2008), pp. 223–242.

[45] A. Sprowitz et al. "Towards dynamic trot gait locomotion: Design, control, and experiments with Cheetah-cub, a compliant quadruped robot". In: *The International Journal of Robotics Research* (2013).

[46] Y. Sugahara, N. Yonezawa, and K. Kosuge. "A Novel Stair-Climbing Wheelchair with Transformable Wheeled Four-Bar Linkages". In: *2010 IEEE Int. Conf. Intelligent Robots and Systems* (2010).

[47] F. Tramacere et al. "Structure and mechanical properties of Octopus vulgaris suckers". In: *Journal of The Royal Society Interface* 11.91 (2014). ISSN: 1742-5689. DOI: 10.1098/rsif.2013.0816.

[48] S. Wang, H. Jiang, and M. R. Cutkosky. "A palm for a rock climbing robot based on dense arrays of micro-spines". In: *Intelligent Robots and Systems, 2016 IEEE/RSJ Int. Conf. on*. IEEE. 2016, pp. 52–59.

[49] R. J. Wood et al. "Microrobot Design Using Fiber Reinforced Composites". In: *Journal of Mechanical Design* 130.5 (2008), p. 052304. ISSN: 10500472. DOI: 10.1115/1.2885509.